

# Astrophysical Tests of Modified Gravity: the Morphology and Kinematics of Dwarf Galaxies

Vinu Vikram, Anna Cabré, Bhuvnesh Jain, Jake VanderPlas

*Department of Physics and Astronomy, University of Pennsylvania, Philadelphia, PA 19104*

*Center for Particle Cosmology, University of Pennsylvania, Philadelphia, PA 19104*

*Astronomy Department, University of Washington, Seattle, WA 98195*

*Department of Computer Science and Engineering, University of Washington, Seattle, WA 98195*

2 November 2018

## ABSTRACT

This paper is the third in a series on tests of gravity using observations of stars and nearby dwarf galaxies. We carry out four distinct tests using published data on the kinematics and morphology of dwarf galaxies, motivated by the theoretical work of Hui et al. (2009) and Jain & Vanderplas (2011). In a wide class of gravity theories a scalar field couples to matter and provides an attractive fifth force. Due to their different self-gravity, stars and gas may respond differently to the scalar force leading to several observable deviations from standard gravity. HI gas, red giant stars and main sequence stars can be displaced relative to each other, and the stellar disk can display warps or asymmetric rotation curves aligned with external potential gradients. To distinguish the effects of modified gravity from standard astrophysical phenomena, we use a control sample of galaxies that are expected to be screened from the fifth force. In all cases we find no significant deviation from the null hypothesis of general relativity. The limits obtained from dwarf galaxies are not yet competitive with the limits from cepheids obtained in our first paper, but can be improved to probe regions of parameter space that are inaccessible using other tests. We discuss how our methodology can be applied to new radio and optical observations of nearby galaxies.

**Key words:** Modified gravity

## 1 INTRODUCTION

The explanation of the observed accelerated expansion of the universe remains a mystery, but possible solutions to this puzzle fall into two broad categories. The first is to posit the existence of a new component of the universe with an appropriate equation of state to cause the observed acceleration. This “dark energy” may be due to an exotic particle or field, or be related to the vacuum energy of space itself. A second approach is to seek to explain this acceleration through modifications to the field equations of general relativity (GR) itself. In recent years this modified gravity (MG) approach has received attention and various approaches have been actively developed – for a review see e.g. Jain & Khoury (2010). Even on theoretical grounds, modified theories of gravity are well motivated: GR is unlikely to be the complete theory of gravity owing to its singularities and non-renormalizability. Hence it is generally considered to be the low energy effective action of some UV-complete theory, though our interest is modifications in the long distance/low energy regime.

A modification of GR on large (astrophysical) scales generically leads to scalar-tensor theories of gravity, where a new scalar field couples to gravity. Equivalently these the-

ories can be described via a coupling of the scalar field to matter, which leads to enhancements of the gravitational force. Nonrelativistic matter – such as the stars, gas, and dust in galaxies – will feel this enhanced force, which in general leads to larger dynamically inferred masses. The discrepancy can be up to a factor of 1/3 in  $f(R)$  or DGP gravity. We note that photons, being relativistic, do not feel the enhanced force, so that lensing measurements probe the true mass distribution.

This enhanced gravitational force should be detectable through fifth force experiments, tests of the equivalence principle (if the scalar coupling to matter varied with the properties of matter) or through the orbits of planets around the Sun (Will 2006). Khoury & Weltman (2004) proposed that nonlinear screening of the scalar field, called chameleon screening, can suppress the fifth force in high density environments such as the Milky Way, so that Solar System and lab tests can then be satisfied. This screening was originally suggested to hide the effects of a quintessence-like scalar that forms the dark energy and may couple to matter – generically such a coupling is expected unless forbidden by a symmetry – so there are theoretical reasons to expect a

screening effect to operate in either a dark energy or modified gravity scenario. Indeed, since there are only a handful of screening mechanisms (Vainshtein and symmetron screening are discussed below), small scale tests of gravity that rely on distinct signatures of screening are useful discriminators of cosmological models.

In this paper we will consider deviations from GR exhibited in theories that rely on chameleon screening. Qualitatively similar behavior occurs in symmetron screening (Hinterbichler & Khoury 2010) and the environmentally dependent dilaton (Brax et al. 2010) and the tests we present here apply to these mechanisms as well<sup>1</sup>.

While local dynamical studies suggest that any fifth-force effects must be screened within the Milky Way, dwarf galaxies in low-density environments may remain unscreened as the Newtonian potential (which determines the level of screening) can be an order of magnitude smaller in magnitude than in the Milky Way. Hence dwarf galaxies can exhibit manifestations of modified forces in their infall motions, internal dynamics and segregation of stars, black holes and gas. Hui et al. (2009), Hui & Nicolis (2010), Jain & Vanderplas (2011), Chang & Hui (2011), Davis et al. (2012) and Jain et al. (2012) discuss various observational consequences. Indeed the small scale dynamics of nearby galaxies may have a bigger signal of MG than large-scale perturbations (see Jain 2011, for a discussion of observational approaches).

In this work, we discuss observable effects on disk galaxies that arise due to their internal dynamics or their interaction with a neighbor or other sources of an external gravitational field. We focus on late-type dwarf galaxies as these are most likely to be unscreened. The observational effects are rooted in the fact that compact objects like stars within the dwarf galaxies can self-screen, and thus respond to a different gravitational potential than the diffuse unscreened components like gas and dark matter. So, for example, if the stellar component of a dwarf galaxy self-screens, it will lag the dark matter and HI gas disk in the infall towards another galaxy. This may lead to a separation of the stellar disk from the center of mass of the dark matter and from the HI disk, and lead to observable distortions of the morphology and/or dynamics of the stellar disk. Jain & Vanderplas (2011) computed a variety of dynamical consequences of these effects.

However, the origin of modified gravity effects may be difficult to disentangle from other astrophysical processes. To address this, we create a control samples of screened galaxies which are not expected to show any of the expected modified gravity effects. By comparing statistics of the unscreened sample and screened control sample, we may derive constraints on modified gravity parameters. The division of observed galaxies into screened and unscreened samples is accomplished based on an estimate of the local value of the external gravitational potential at the location of each galaxy: see Cabré et al. (2012) for a description of the methodology used to distinguish the screened and un-

screened samples. Jain et al. (2012) used this methodology and obtained modified gravity constraints based on cepheid variable stars and other distance indicators. This paper is the third in the series of papers on astrophysical tests of gravity:

In this paper we perform several of the proposed tests of modified gravity using currently available data. Because of the low signal-to-noise of these types of tests, a large amount of high quality data will be required to obtain competitive constraints on modified gravity models. Therefore, one of the main goals of this paper is to show the strengths and weaknesses of currently available data for these tests, and explore the requirements for future data in this area.

This paper is organized as follows. In section 2 we describe the method to generate potential map of the local Universe, which allows us to prepare our samples of screened and unscreened galaxies. In section 3 we briefly summarize each of the observable effects we will use to test modified gravity. In section 4 we describe the offset between stellar and gaseous components, which includes: offset between HI and optical centroids (section 4.1), offset between optical center and H $\alpha$  center (section 4.2), and offset between red giants and main sequence stars (section 4.3). In section 5 we study MG-induced warping of edge-on galaxies. In section 6 we describe the tests based on gaseous velocity rotation curves, which includes HI - H $\alpha$  velocity differences (section 6.1), and asymmetry in the H $\alpha$  curves (section 6.2). We conclude in section 7.

## 2 POTENTIAL MAP OF THE LOCAL UNIVERSE

Each of the modified gravity tests presented in this paper relies on comparing various observationally-derived statistics of a screened and unscreened sample of galaxies. Therefore, the first step of the analysis is to determine whether each galaxy in our sample is likely to be screened, i.e. the ‘fifth’ force due to the scalar field is suppressed by the deep potential well of the galaxy or its environment. Because the screened sample should be free of any fifth-force effects, we use it as a control sample. The detailed procedure for determining screening has been described and tested via N-body simulations of  $f(R)$  gravity in Cabré et al. (2012); we summarize these results here.

For an isolated spherical halo in  $f(R)$  gravity, the chameleon effect is suppressed if  $f_{R0} \leq 2/3 |\phi_N|/c^2$ , where  $\phi_N$  is the Newtonian potential of the object (Hu & Sawicki 2007). We will approximate galaxies as isolated spherical halos, and make use of this condition to determine whether an object is self-screened or environmentally screened: i.e. we look for the galaxies which satisfy the following conditions:

$$\frac{|\phi_{\text{int}}|}{c^2} > \frac{3}{2} f_{R0} \quad \text{or} \quad \frac{|\phi_{\text{ext}}|}{c^2} > \frac{3}{2} f_{R0} \quad (1)$$

The first condition describes the *self-screening* condition, with  $|\phi_{\text{int}}| = GM/r_{\text{vir}}$ , where the  $M$  and  $r_{\text{vir}}$  are the mass and virial radius. We typically use measurements of the circular velocity at large radii to establish self-screening, since we work with rotating disk galaxies for our tests. The second condition describes *environmental screening* condition, with  $|\phi_{\text{ext}}|$  representing the Newtonian potential due to the

<sup>1</sup> In order to identify the screened and unscreened galaxies it is necessary to calibrate on N-body simulations, which give different criteria for different screening mechanisms. While we do not implement criteria for any mechanism other than chameleon, our results appear robust to the details of screening.

neighbor galaxies within the background Compton length  $\lambda_C$ . The external potential  $|\phi_{\text{ext}}|$  is evaluated using neighboring galaxies as:

$$|\phi_{\text{ext}}| = \sum_{d_i < \lambda_C + r_i} \frac{GM_i}{d_i} \quad (2)$$

where  $d_i$  is the physical distance to the neighboring galaxy with mass  $M_i$  and virial radius  $r_i$ .  $\lambda_C$  is related to the background field value  $f_{R0}$  (Schmidt et al. 2009):

$$\lambda_C \approx 32 \sqrt{\frac{|f_{R0}|}{10^{-4}}} \text{Mpc} \quad (3)$$

Identifying screened and unscreened regions requires knowledge of the masses and three-dimensional positions of all the objects in the sky. Since our knowledge is limited by finite survey sizes and depths, we assume that most of the contribution to the environmental screening potential comes from clusters and groups of galaxies. This is a reasonable assumption as the potential of a rich cluster is up to two orders of magnitudes larger than a typical galaxy. Cabré et al. (2012) compiled a catalog of bright clusters with known redshifts based on Abell (Abell et al. 1989) and ROSAT (Ebeling et al. 1996) observations. We remove many clusters from the Abell catalog as they lack spectroscopic redshift or have redshift greater than 0.1. Our final catalog contains 675 clusters of galaxies with galactic latitude  $|b| > 20$ .

The next most significant contribution comes from galaxy groups. Yang et al. (2007) provides a nearly complete catalog of groups in the SDSS region, including around 400,000 galaxies covering the redshift range 0.01 – 0.2. In addition, we use the group catalog from the 2M++ all sky survey (Lavaux & Hudson 2011) to create a combined catalog of 153380 SDSS and 3984 2M++ galaxy groups. The final contribution to the catalog are local galaxies within 10 Mpc, identified by Karachentsev et al. (2004).

With this catalog in place, an estimate of the mass of each object is required in order to calculate the potential. We determine the mass using either the mass-luminosity relation given by Reiprich & Böhringer (2002) or the mass-velocity dispersion relation given by Evrard et al. (2008). The masses of SDSS groups and local galaxies are taken directly from Yang et al. (2007) and Karachentsev et al. (2004), respectively<sup>2</sup>.

Using the mass of the clusters, groups and galaxies, we generate a potential map of the sky. In this paper we use values of the Compton length between  $\lambda_C = 3.2$  Mpc and  $\lambda_C = 1.0$  Mpc corresponding to  $f_{R0}$  parameters  $10^{-6}$  and  $10^{-7}$ . Due to survey incompleteness, the derived potential map is only an approximation for many regions of the sky. This could potentially lead to systematic inaccuracies in labeling of screened and unscreened objects. A detailed discussion of these uncertainties can be found in Cabré et al. (2012).

<sup>2</sup> Note that Karachentsev et al. (2004) reports the mass for only 313 of the 451 galaxy sample. See <http://www.sas.upenn.edu/~vinu/screening/index.html> for an extensive description of the catalog.

### 3 OBSERVABLE EFFECTS MODIFIED GRAVITY

In chameleon gravity theories, objects with large gravitational potential may be self-screened (see Eq. 1). This may lead to observable differences in the dynamics of different galactic components: the gaseous disk, dark matter halo, and giant stars may feel the fifth force, while the self-screened main sequence stars move according to standard gravitational dynamics. The different forces on these components lead to several potentially observable morphological and kinematical differences between the two components. In this section, we summarize the expected effects of the fifth force, as well as potential observational tracers of these effects.

#### 3.1 Summary of physical effects of modified gravity

The following effects of modified gravity are expected to appear in unscreened dwarf galaxies. Quantitative estimates of the magnitude of these observables are given in the following sections. For more details and motivation of these predictions, see Jain & Vanderplas (2011).

(i) **Offset between stellar and gaseous components (section 4):** Chameleon theories predict that in the presence of a suitable potential gradient, low density, unscreened components like dark matter or neutral hydrogen clouds (HI) will fall faster along an external potential than will self-screened stars. This difference in acceleration may cause a measurable offset between the centroid of the stellar disk and the gaseous disk. The population of red giant stars, being partially screened, may also show an observable offset from the population of main sequence stars. The size of the offset depends strongly on the mass and concentration of the dwarf galaxy’s halo, as well as the distance to neighboring galaxies. Jain & Vanderplas (2011) estimate this offset may be several percent of the virial radius of suitable dwarf galaxies. We carry out three tests of such offsets in section 4.

(ii) **Warping of the stellar disk (section 5):** As the halo moves along an external potential gradient, it pulls at the lagging stellar component. If the potential gradient is aligned with the axis of rotation, the steep slope of the halo potential may introduce a U-shaped warp in the stellar disk. The shape and strength of the warp depends on the mass profile of the dwarf galaxy halo, as well as the strength of the external potential gradient. The warp is expected to align with this potential gradient. Jain & Vanderplas (2011) estimate the warp to be of order 0.1 kpc, though it varies significantly depending on the external fifth force acting on the dwarf galaxy.

(iii) **Rotation curve tests (section 6):** If a disk galaxy falls edge-on, or more generally if the external potential gradient is not aligned with the galaxy’s axis of rotation, the offset between stellar and halo centers can perturb the stellar disk and cause an asymmetry in the stellar rotation curve. This is due to the fact that the dominant force on the stellar disk is from the potential of the halo, rather than the potential of the disk itself. The asymmetry can be as high as 10 km/s. The asymmetry can be distinguished from standard astrophysical sources by comparing the stellar disk with the gaseous disk. A version of this test is show in section 6.2.

In principle the rotation velocity of an unscreened gaseous disk is also enhanced relative to the stellar disk by a factor of  $\sqrt{1 + \Delta G/\bar{G}}$ , where  $\Delta G$  is the contribution of the fifth force to the self-gravity of a galaxy (Hui et al. 2009). We find that current data is unsuitable to carry out this test: see section 6.1 for a discussion of current data and its limitations.

In isolated cases, any of the above observable properties could potentially be explained via standard astrophysical effects. But under modified gravity we would expect to see multiple effects in conjunction, and to see offsets and warps aligned with the direction of the external gravitational force. More importantly, we expect these effects to be more prevalent in unscreened galaxies than in screened galaxies: such a correlation would be difficult to explain using conventional explanations, such as bars, spiral arms, asymmetric drift, and external tidal effects. In the following sections, therefore, we explore aggregate statistics relating to the presence of these observable effects in screened and unscreened populations.

### 3.2 Observational Tracers

In order to trace gaseous components of dwarf galaxies, we use observations of the 21 cm line which results from the hyperfine transition of neutral hydrogen. In order to trace the stellar component, we use the distribution of optical light. Traditionally,  $H\alpha$  is also used as a kinematical tracer of the disk, but this presents some complications for studies of modified gravity.

$H\alpha$  emission in dwarf galaxies arises because the high energy radiation from stars ionizes the neutral gas in the ISM, forming a ‘‘Stromgren Sphere’’. As the ions within this region recombine, the photons emitted in the  $n = 3 \rightarrow n = 2$  transition of Hydrogen lead to the  $H\alpha$  emission line.

Historically, this line has been used to measure the stellar rotation curve, and is expected to give accurate measurements of the dynamics of the stellar disk in the absence of modified gravity. However, the possibility of a fifth force which affects stars and gas calls this expectation into question. Recall that the star is screened by its own potential, but this potential may not be strong enough to screen the whole of the surrounding sphere.

A rough calculation shows that for a star of mass  $10M_{\odot}$  and radius  $5R_{\odot}$ , the surface potential is  $\sim 4 \times 10^{-6}$ . Therefore, this star will be screened for background field value less than  $4 \times 10^{-6}$ . For  $f_{R0} = 1 \times 10^{-6}$  ( $2 \times 10^{-7}$ ), this potential is only sufficient to screen ionized gas within  $4.6 \times 10^{-7}$  ( $2.3 \times 10^{-6}$ ) parsec of the star – that is, about 4 (20) times the star’s radius. For typical HII regions which have radii of order 10pc, the region screened by the stellar potential is negligible. Therefore, we would expect that the HII region feels the fifth force and orbits faster than the associated star – this raises interesting questions about what fraction of stars remain associated with significant HII regions. Thus, under the assumptions of modified gravity, it is not safe to assume that  $H\alpha$  traces the dynamics of the stellar component. We will simply assume that  $H\alpha$  is a gaseous tracer and leave a detailed study for later work, though we provide a brief empirical test Section 6.1.

A better tracer of the rotation of the stellar component under modified gravity may be molecular absorption lines

in the stellar spectra, which arise much closer to the star. Absorption lines such as MgIb or CaII would trace the stellar rotation curve accurately under both modified gravity and general relativity. However, these lines are difficult to observe, particularly in the low-surface-brightness outskirts of the galaxy.

## 4 OFFSET BETWEEN STELLAR AND GASEOUS COMPONENTS

In this section we consider three tests based on the first observable effect: the expected offset between unscreened and self-screened components of the unscreened galaxy sample. Simple calculations indicate that under reasonable approximations, this offset should be large enough to be observable (Jain & Vanderplas 2011). We consider three potential avenues toward this observation below.

### 4.1 Offset between HI and optical centroids

We first compare the optical centroid, which traces the stellar component, to the centroid of HI gas measured via its 21cm emission. Here the optical observations are taken from the SDSS  $r$ -band (Abazajian et al. 2009) while the HI centroids are taken from the ALFALFA survey which used the Arecibo radio telescope (Giovanelli et al. 2005, 2007; Sain tonge et al. 2008; Kent et al. 2008; Martin et al. 2009). The astrometric precision (about 24 arcseconds) of these observations are limited by the relatively large beam size of the radio maps. Though the low resolution of the HI image makes any offset difficult to measure for a single image, the statistical uncertainty can be reduced by considering a large sample of galaxies.

To reduce the uncertainty in the spatial centroiding, we limit our sample to those galaxies within 40 Mpc. To minimize the error introduced by the incompleteness in our catalog described in Section 2, we further restrict our analysis to the SDSS region, where we have information on galaxy groups down to a mass of  $5 \times 10^{11}M_{\odot}$ . Finally, to limit the effects of different detection thresholds between the SDSS and Arecibo images, we keep only the galaxies whose optical and HI centroids are within 1 arcmin. After these cuts are made, the resulting catalog contains 245 dwarf galaxies.

In order to identify galaxies which are large enough to be self-screened, we use the maximum velocity estimated from W50, i.e. the velocity width of the source line profile measured at the 50% level of each of the two peaks. This was corrected for instrumental broadening by the ALFALFA team. However, this must be further corrected for turbulence and inclination. The turbulence correction was performed according to Tully & Fouque (1985) using an average velocity dispersion in the gas component of 8 km/s (Begum et al. 2006; Geha et al. 2006). Finally, we apply the inclination correction based on the observed axis ratio  $q$  in the SDSS  $r$ -band. The maximum velocity is found via:

$$v_{\max} = \frac{W50_c}{2\sqrt{1 - q^2}}, \quad (4)$$

where  $W50_c$  is the turbulence corrected W50 and  $q$  is the axis ratio of the galaxy. For a background field value  $f_{R0}$ ,

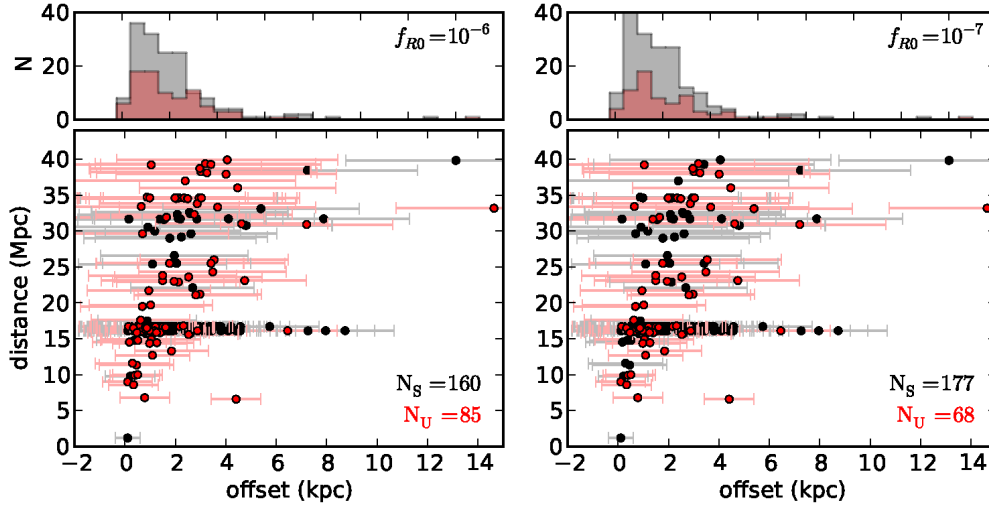


**Figure 1.** The distribution of the measured offset between the HI and optical centroids for galaxies observed by the ALFALFA and SDSS surveys. The black (red) points represent screened (unscreened) galaxies for model parameter values  $f_{R0} = 1 \times 10^{-6}$  (left panel) and  $f_{R0} = 2 \times 10^{-7}$  (right panel)

the unscreened galaxies satisfy (see Jain et al. 2012)

$$\left(\frac{v_{\max}}{100}\right)^2 \lesssim \frac{f_{R0}}{2 \times 10^{-7}}. \quad (5)$$

The above criteria yields 68 (85) unscreened and 177 (160) screened galaxies for  $f_{R0} = 2 \times 10^{-7}$  ( $f_{R0} = 10^{-6}$ ).

In Figure 1 we show the measured HI/optical offset for samples of different screening level, along with the distributions of offsets for two values of  $f_{R0}$ . The errors shown are estimated from the 24 arcsec centroid error of the radio maps, converted to a physical distance using the distance to each galaxy.

The interpretation of any observed offset is made difficult by the fact that there are several potential astrophysical (non-MG) sources of separation, as well as the fact that we cannot predict the magnitude or direction of the MG-induced separation. We address this by proposing an aggregate statistical model of the data, which takes into account the expected difference between the screened and unscreened samples.

To account for non-MG related separation, we assume that standard astrophysical effects will produce a scatter in the distribution of projected HI-optical separations centered at zero and with a standard deviation  $\sigma_{GR}$ . This scatter will be present in both the screened and unscreened samples. To account for MG-related separation, we assume that within the unscreened sample, there will be an additional Gaussian scatter centered at zero with standard deviation  $\sigma_{MG}$ . Then the observed separation for a screened galaxy and an unscreened galaxy is respectively

$$\begin{aligned} \hat{s}_i^{scr} &= abs(s_i^{scr}) + \varepsilon_i \\ \hat{s}_i^{unscr} &= abs(s_i^{unscr}) + \varepsilon_i \end{aligned} \quad (6)$$

where  $\hat{s}_i^{scr}$  and  $\hat{s}_i^{unscr}$  are the observed offsets for the screened and unscreened samples, and  $s_i^{scr}$ ,  $s_i^{unscr}$ , and  $\varepsilon_i$  are (unobserved) values drawn from Gaussian distributions:

$$s_i^{scr} \sim \mathcal{N}(0, \sigma_{GR}^2)$$

$$s_i^{unscr} \sim \mathcal{N}(0, \sigma_{GR}^2 + \sigma_{MG}^2)$$

$$\varepsilon_i \sim \mathcal{N}(0, \sigma_i^2) \quad (7)$$

where  $\mathcal{N}$  denotes a Gaussian distribution and  $\sigma_i$  is the (known) measurement error associated with observation  $i$ .

With this model in place, we can find the most likely parameter combination within a Bayesian formalism, by writing

$$\begin{aligned} p(\sigma_{MG}, \sigma_{GR} | \{\hat{s}_i\}) &\propto p(\sigma_{MG})p(\sigma_{GR}) \left[ \prod_{i \in S^{scr}} g(\hat{s}_i; 0, \sigma_{GR}^2 + \sigma_i^2) \right] \\ &\times \left[ \prod_{j \in S^{unscr}} g(\hat{s}_j; 0, \sigma_{MG}^2 + \sigma_{GR}^2 + \sigma_j^2) \right] \end{aligned} \quad (8)$$

where  $g(x; \mu, \sigma^2)$  is the Gaussian probability distribution with mean  $\mu$  and width  $\sigma$ ;  $p(\sigma_{MG})$  and  $p(\sigma_{GR})$  are the priors on the parameters; and  $S^{scr}$  and  $S^{unscr}$  are respectively the sets of screened and unscreened observations.

In Figure 2 we show the 1-, 2-, and 3- $\sigma$  contours of the posterior distribution given in Eq. 8 as a function of  $\sigma_{MG}$  and  $\sigma_{GR}$ . The left panel shows the result for the observed data: this data is not precise enough to rule-out a  $\sim 1$ kpc scatter due to modified gravity: this is primarily due to the large observational error in the measurement of the radio centroid. In the right panel, we see that if the aggregate astrometric accuracy were to be improved by a factor of 10 (i.e. a 2.4 arcsecond centroid accuracy, or a factor of 100 increase in the sample size, or some combination of these two improvements), the observations would be sensitive enough to detect a scatter due to modified gravity of  $\sim 0.5$ kpc, on the order of the offsets predicted by (Jain & Vanderplas 2011) for typical MG theories.

One important detail of these results for such low signal-to-noise data is their dependence on the precise determination of the measurement uncertainty. Within the model given by Equation 8, the measurement error is degenerate

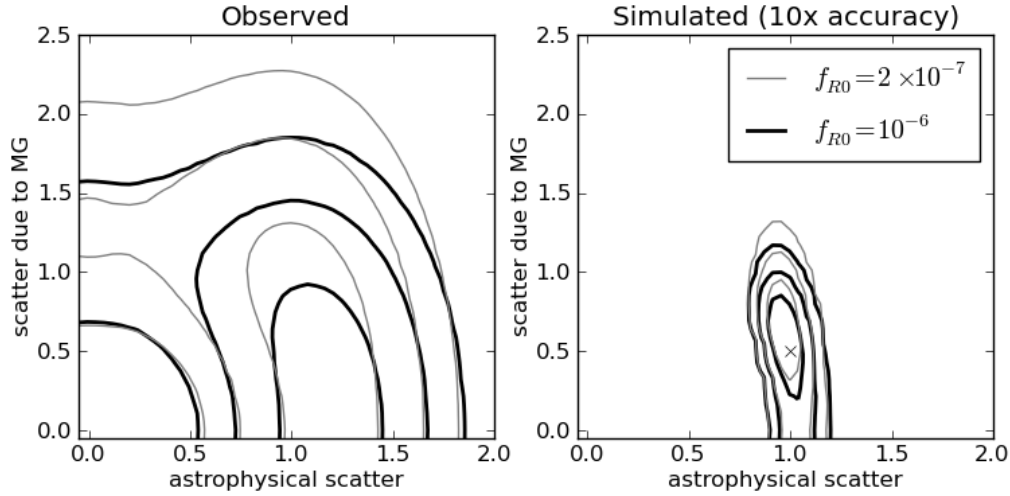


**Figure 2.** The 1-, 2-, and 3- $\sigma$  contours for the scatter in observed HI/optical centroid separations in nearby dwarf galaxies. The left panel shows the results given the observed sample of 245 dwarf galaxies described in §4.1. Because of the large beam size of the radio maps, the data cannot distinguish between modified gravity and general relativity. The right panel shows a simulated sample drawn from the model with a scatter due to modified gravity of 0.5 kpc (indicated by the 'X'), with a factor of ten improvement in astrometric precision (or a combination of improved astrometry and larger sample size). The resulting posterior can distinguish the predicted effects of modified gravity at the 1- $\sigma$  level.

with the astrophysical offset: any increase in assumed measurement error will be offset by a commensurate decrease in the astrophysical scatter at maximum likelihood. Furthermore, because the uncertainty of the measurement dominates the signal by a factor of up to 4 for each galaxy, even a 10% overestimate or underestimate in the centroid error will lead to significant differences in the maximum likelihood fit. This caveat should be kept in mind when interpreting Figure 2.

Thus, while the current data are not precise enough to either confirm or rule-out modified gravity theories, a large, combined radio/optical survey of nearby dwarf galaxies with very precise and well-characterized astrometry could provide strong constraints on typical modified gravity theories.

#### 4.2 Offset between optical center and H $\alpha$ kinematical center

A primary weakness of the measurements explored in the previous section is the astrometric precision of centroid measurements in the radio. In this section we measure the same effect, but using the kinematical center of the H $\alpha$  disk as a tracer of its centroid. Here we assume that the gas producing the H $\alpha$  line is unscreened and traces the dark matter, which means that the rotation curve should (in principle) have the same center as the dark matter halo (see Sec 3.2). As above, we search for systematic offsets between the (self-screened) stellar component and this (unscreened) gaseous component.

For this section, we use data presented by Persic & Salucci (1995): they re-analyze 967 H $\alpha$  velocity rotation curves originally observed by Mathewson et al. (1992), and publish the offset between the kinematical center (which symmetrize the rotation curve) and the optical center. We divide these galaxies into a screened and unscreened sample

using the methodology presented in Section 2, leading to 25 (690) unscreened galaxies and 858 (193) screened galaxies for  $f_{R0} = 2 \times 10^{-7}$  ( $f_{R0} = 10^{-6}$ ).

In the left panel of Figure 3, we show the distance to each galaxy along with its mass indicator, the maximum rotation velocity. The mild correlation between these measurements can be traced to observational bias: smaller, fainter galaxies are less likely to be observed at larger distances. Note that velocities range from 50 to 300 km/s, which allow us to test theories from  $f_{R0} = 10^{-6}$  (galaxies self-screened if  $v_{\max} > 225$  km/s) to  $f_{R0} = 10^{-7}$  ( $v_{\max} > 70$  km/s). The color of each point indicates whether the galaxy is screened at a level of  $f_{R0} = 10^{-6.5}$ . There is a relatively sharp boundary between the screened and unscreened samples seen at  $\sim 120$  km/s rotation velocity: this is due to the self-screening criterion met by larger-mass galaxies.

Because the size of the expected MG displacement scales with the size of the dark matter halo (Jain & Vanderplas 2011), we work here with the relative offset  $\delta = s_{\text{obs}}/r_{\text{opt}}$  where  $s_{\text{obs}}$  is the offset between the optical and kinematical centers and  $r_{\text{opt}}$  is the optical radius of the galaxy. This relative offset does not show an obvious correlation with galaxy rotation velocity, as can be seen in the right panel of Figure 3.

To search for indications of modified gravity, we use the aggregate likelihood formalism developed in the previous section, replacing the absolute deviations  $s$  with the relative deviations  $\delta$ . The resulting posterior is shown in Figure 4. In comparison to the ALFALFA results in Figure 1, the data posterior is much tighter: this is mainly due to the increased astrometric accuracy of these measurements.

The left panel of Figure 4 shows results for the entire sample, and (for  $f_{R0} = 10^{-6}$ ) indicates an approximately 1- $\sigma$  detection of an offset due to modified gravity. Because this result uses the whole sample, however, it is potentially

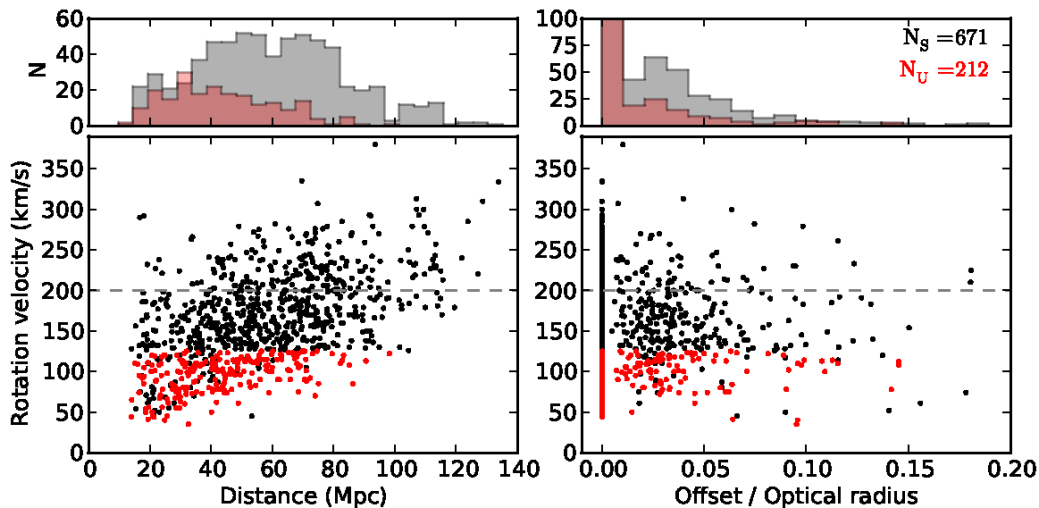


**Figure 3.** The distribution of galaxies used for the optical/kinematic offset test described in Sec 4.2. The left panel shows the distance and maximal rotation velocity (a tracer of mass) of the galaxy sample; the right panel shows the relative offset between the gaseous and stellar components. Black (red) points represent screened (unscreened) galaxies at  $f_{R0} = 10^{-6.5}$ . The clear mass dependence of the screening condition is due to self-screening of massive galaxies.

biased by the sizes of the galaxies in the sample. As shown in Figure 3, the vast majority of screened galaxies in our sample are not environmentally screened, but self-screened. The differential offset shown in this analysis, then, not only reflects the difference between screened and unscreened galaxies, but also the difference between large and small galaxies. Even absent modified gravity effects, we may expect statistically significant differences in observed offsets between these samples.

To limit the effect of this size bias, we repeat the analysis, limiting our galaxy sample to those with a maximum rotation velocity less than 200 km/s (i.e. those galaxies below the dashed line in Figure 3). Having controlled for this bias, we see in the left panel of Figure 4 that the offsets are consistent with General Relativity for both screening levels.

Still, this analysis does not rule out offsets due to modified gravity with a scatter of approximately 2% of the optical radius of the galaxy. Under ideal conditions, Jain & Vanderplas (2011) showed that the expected offsets for typical modified gravity theories could be as high as 10% the optical radius of the galaxy. This predicted offset decreases as the size of the galaxy increases, and as the distance to the neighboring galaxy increases. Thus a 2% upper-limit is not enough to definitively rule-out modified gravity theories.

### 4.3 Offset between centroids of red giants and main sequence stars

In modified gravity scenarios, red giant stars present an interesting case: their cores may be dense enough to self-screen, while their diffuse outer shells remain unscreened and feel the fifth force. This partial screening can lead to interesting effects: for example, Chang & Hui (2011) have recently shown that red giant stars evolve differently under modified gravity compared to main sequence stars, and that

this difference can be used to constrain modified gravity theories.

In this section we make use of red giant populations to constrain modified gravity in a different way: just as unscreened gas and dark matter will separate from the screened main sequence stars in the presence of an external potential gradient, partially screened red giants will be expected to separate from the population of main sequence stars as well.

#### 4.3.1 Data and centroid estimation of RGB and main sequence stars

Recently, Dalcanton et al. (2009) published positions and magnitudes of individual stars within 69 nearby dwarf galaxies (distance < 4 Mpc,  $|b| > 20$  deg)<sup>3</sup>. Absolute magnitudes of these galaxies ( $M_B$ ) range from -20 to -8. They observed nearly  $10^3$  to  $10^5$  stars in each galaxy. In our study we need full images of the galaxies to estimate the displacement between RGB (red giant branch) and main sequence stellar populations as partial images of galaxies introduce artificial displacement between those two populations. We use only those galaxies which pass this criterion. In addition, we exclude all the galaxies in which foreground contamination leads to poorly-defined red giant branches. Finally, we include galaxies only if they have at least 3000 observed stars. The final sample consists of 28 galaxies: under either screening assumption ( $f_{R0} = 10^{-6}$  and  $f_{R0} = 10^{-7}$ ) every galaxy is unscreened, which means this test cannot rely on a screened control sample.

For each galaxy, we select red giants from the color-magnitude diagram. In Figure B1 we show an example of red giant star selection. Because the fifth force acts only on the outer regions of the largest giant stars, we tune the cutoff to select only the brightest, and therefore the largest, of the

<sup>3</sup> See <http://www.nearbygalaxies.org>

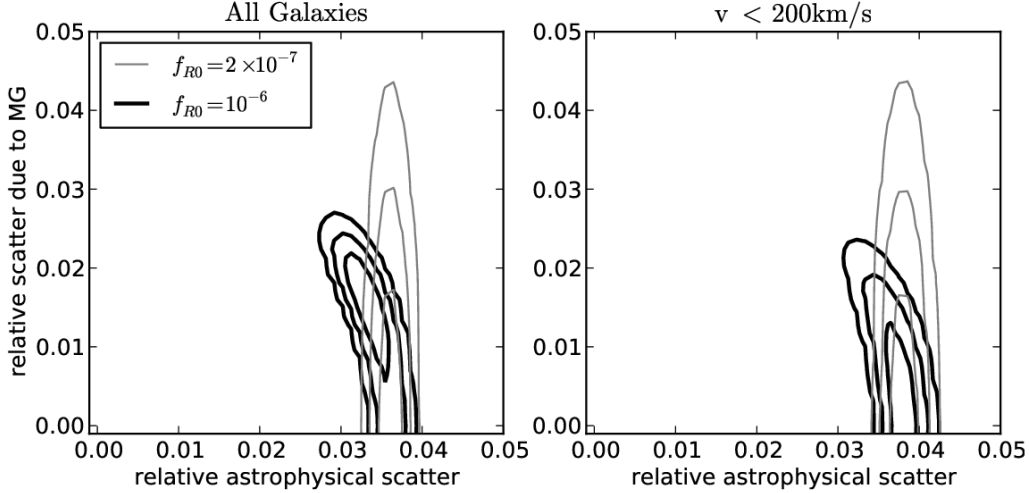


**Figure 4.** The Bayesian estimate of the contributions of MG and astrophysical effects to the offset between kinematical and optical centroids (see discussion of this model in Sec 4.1). The left panel shows a mildly significant offset due to modified gravity: we argue that this is due to the bias of the screened sample toward high masses. After controlling for this by removing galaxies with rotation greater than 200 km/s, the estimate is consistent with GR.

red giant stars. Next we define the area of the galaxy within which the centroid will be calculated. This is done by taking isocontours of stellar number density significantly above the noise level. Errors in the centroids of the red giant and main sequence populations are calculated using bootstrap resampling with 50 realizations. These are shot-noise dominated. Since the number of red giants is at least an order of magnitude lower than the number of main sequence stars, the error in the centroid displacement is dominated by the error in the centroid position of the red giant sample.

#### 4.3.2 Estimation of the external fifth force

Because of the lack of control sample, detecting modified gravity here depends on correlating the direction of displacement with the strength and direction of the background gravitational potential gradient at each dwarf galaxy due to its neighbors. In order to estimate this, we use the catalog of nearby galaxies given by Karachentsev et al. (2004). This catalog is nearly complete out to a distance of 10 Mpc and it contains a total of 431 galaxies with known mass for 313 galaxies. We fit a linear relation between the mass and magnitude (in logarithmic scale) to the galaxies with known mass and use this empirical relation to estimate the masses of the remaining galaxies. By using distances and masses of neighboring galaxies we can construct the force vector (per unit mass) as

$$\vec{a} = \sum_{i \in \text{unscr}} \frac{GM_i}{|\vec{r}_i - \vec{r}|^2} \frac{\vec{r}_i - \vec{r}}{|\vec{r}_i - \vec{r}|} \quad (9)$$

where  $m$  is the studied galaxy mass at position  $\vec{r}$ ,  $M_i$  the mass of the neighbor  $i$ , which is at position  $\vec{r}_i$  and  $G$  is Newton's constant. The sum includes only unscreened neighbors at a distance below the Compton length. The gravitational

potential  $W$  can be calculated as

$$W = \sum_i \frac{GM_i}{|\vec{r}_i - \vec{r}|} \quad (10)$$

where the sum includes all neighbors at a distance below the Compton length. Here we use the potential to estimate the magnitude and direction of the background gravitational force, as well as to estimate the potential to define the screening level for the dwarf galaxy sample. The force has some errors due to the uncertainty in distance (5%) and mass ( $\sigma_{\log(M)} = 0.2$ ). In our case, uncertainty in mass is the dominant source of error.

#### 4.3.3 Results and comparison with theory

In Figure 5 we plot the displacement of red giants from main sequence stars projected to the external force vector as a function of the force per unit mass. The force vector is previously projected to the plane of the sky perpendicular to the line of sight. In order to calculate the error in the projected displacement, we take into account both the error in the centroids and the error in the vector force, and show the results for  $f_{RO} = 10^{-6}$  and  $f_{RO} = 10^{-7}$ . There is no statistically significant correlation between the force and projected displacement. The weighted average displacement in the direction of the external force for  $f_{RO} = 10^{-6}$  ( $f_{RO} = 10^{-7}$ ) is  $-10.2 \pm 5.5$  pc ( $-4.7 \pm 6.4$  pc), consistent with zero to within  $2\text{-}\sigma$  ( $1\text{-}\sigma$ ). The errors on these estimates include intrinsic dispersion, as explained in Appendix A.

In Figure 6 we compare the projected displacement to the prediction, given the external force and assuming a cored isothermal sphere (see Equation 2.3 of Jain & Vanderplas (2011) for the analytical expression of the offset). The prediction takes into account errors in the masses and distances of neighboring galaxies, as well as errors in the determination of the galaxy mass, core radius, and core mass. The last



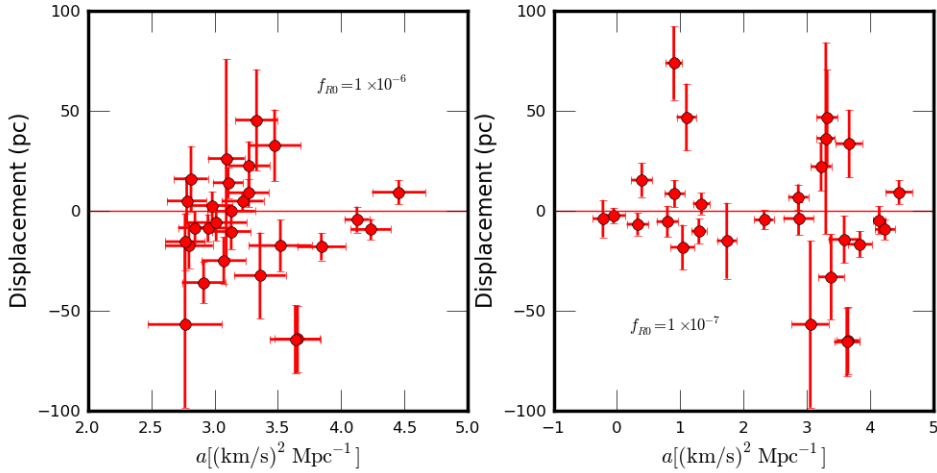


**Figure 5.** The displacement of red giants from main sequence stars projected along the external fifth force from a sample of 28 nearby dwarf galaxies. The displacement is plotted as a function of the external force per unit mass (Eq. 9). In the left (right) panel, we set  $f_{R0} = 10^{-6}$  ( $10^{-7}$ ). All the galaxies are unscreened. There is no significant correlation between the displacement and the applied force. The mean displacement in the direction of the external force is  $-10.2 \pm 5.5$  pc and  $-4.7 \pm 6.4$  pc for the two cases, consistent with GR.

two quantities are estimated using the strong empirical correlation between virial mass and core radius and core mass (Swaters et al. 2003, 2011). We have assumed  $\Delta G/G = 1$  for the predictions, but this result can be easily scaled for other values of  $\Delta G/G$ . The mean difference between the observed displacement  $d$  and predicted displacement  $p$  is  $p - d = 12.5 \pm 6.1$  pc ( $-0.7 \pm 4.8$  pc) for  $f_{R0} = 10^{-6}$  ( $10^{-7}$ ).

We find that both these tests are unable to rule-out either GR or modified gravity. The main reason for this lack of discriminatory power is because most of the galaxies are very isolated, so the external force has a small magnitude. In Appendix B we discuss in detail a series of important systematic uncertainties involved in this test.

#### 4.3.4 Future directions

We find that tests of modified gravity through comparison of the positions of red giant and main sequence stars are inconclusive, mainly owing to the error associated with the small sample size. Also, because red giants are only partially screened, the signal may be diluted when compared to the tests of the previous sections. Additionally, the lack of a control sample means that the uncertainty in the external force is the limiting factor if one wants to constrain modified gravity with only the unscreened sample as such tests require much better prediction to compare the data.

Future studies making use of this effect should focus on unscreened galaxies with very close neighbors, which will thus experience stronger external potential gradients, and drive the separation to more detectable levels. It would also be helpful to focus on similarly-sized screened galaxies to provide a control sample (though this pursuit may be limited by the relative paucity of nearby screened dwarf galaxies). The best approach would be to focus on a limited number of galaxies with regular morphology, to reduce intrinsic systematic effects, with a very well defined external force.

Another potentially interesting method for this sort of measurement would be to use integral field spectra of galax-

ies and estimate the red giant and main sequence contributions to the spectrum as a function of position: any systematic offset, aligned with the external fifth force in the inferred mass of red giant and main sequence stars could indicate the presence of a fifth force acting on the red giant population.

## 5 WARPING OF EDGE-ON GALAXIES

In the previous section, we discussed the expected offset of the stellar and dark matter components of suitable unscreened dwarf galaxies within modified gravity. As shown in Jain & Vanderplas (2011), this offset may lead to an observable morphological signature: a bowl-shaped warp in the stellar disk, aligned with the direction of the external gravitational force and this effect will be maximized when the gravitational force is perpendicular to the plane of the disk. When viewed edge-on, this will result in a symmetric U-shaped warp in the disk of the infalling galaxy. Because standard astrophysical dynamics (e.g. tides) could lead to similar effects, we use screened galaxies as a control sample and look for a statistically significant higher fraction of such U-shaped warps in the unscreened sample.

### 5.1 Data and estimation of warp parameter

We search for warps in low mass, nearly edge-on galaxies using the ALFALFA and SDSS data. The rotation velocity measured by the former is used to find self-screened galaxies, and images from the latter are used to estimate the galaxy warp. Because warp is difficult to observe in face-on galaxies, we limit our sample to those galaxies with an axis ratio of less than 0.6. In the resulting sample of 495 galaxies, 128 (59) galaxies are screened and 367 (158) unscreened, for a Compton scale length of 3 (1) Mpc which corresponds to  $f_{R0} = 1 \times 10^{-6}$  ( $f_{R0} = 2 \times 10^{-7}$ ). For  $f_{R0} = 2 \times 10^{-7}$  we use only galaxies with  $v_{\max} < 200$  km/s in the screened sample.

In order to reduce the type of mass-related systematic

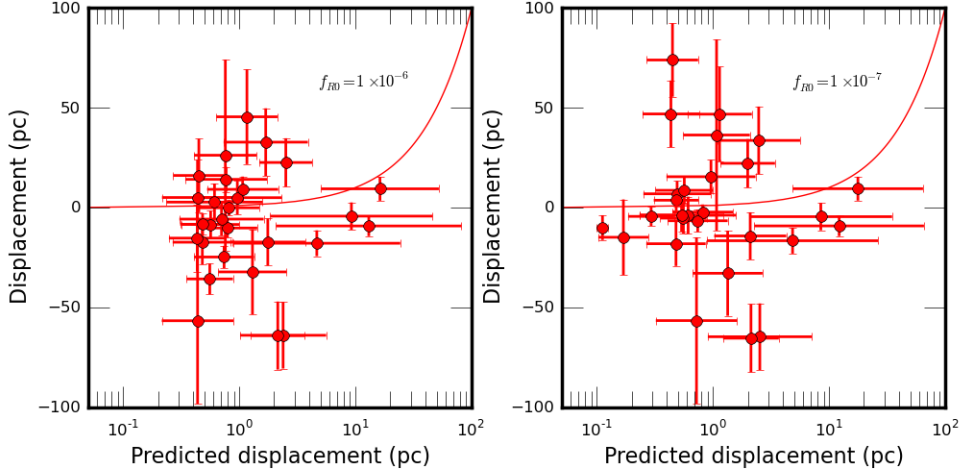


**Figure 6.** The estimated projected displacement, as in Fig. 5, is compared with the predicted displacement assuming  $\Delta G/G = 1$ . In the left (right) panel, we set  $f_{R0} = 10^{-6}$  ( $10^{-7}$ ). The solid line shows the one to one correspondence. It is evident that while the observations are consistent with GR, one cannot rule out modified gravity given the large errors in the predictions and systematics.

effects discussed in the previous section, we include only smaller galaxies in which the self-screening condition (Eq. 5) does not apply: the separation of screened and unscreened galaxies is based only on the environment. The warp of the galaxies is found by slightly modifying the method used in Jiménez-Vicente et al. (1997): after sky subtraction, we first rotate the SDSS images so that the major axis of the galaxies align with the horizontal axis. The center of rotation is found using the SExtractor package (Bertin & Arnouts 1996). We mask stars and other contaminating nearby objects in the image. After removing all the contaminating objects and pixels in the frame we find the centroids for each column in the image by fitting a Gaussian to the column and taking the first moment. This leads to a ‘warp curve’, i.e. the centroid of the columns as a function of distance from the center of the galaxies. To clean the curve, we start from the center of the galaxy and sweep through the curve, omitting any column which has a linearly-interpolated centroid that deviates more than three pixels from that of the previous column. An example of such a cleaned warp curve is shown on Figure 7.

After estimating the warp curve, we quantify the overall warp by defining the following two measures:

$$w_1 = \frac{\int_0^L \frac{x}{L} \frac{y}{L} \frac{dx}{L}}{\int_0^L \frac{x}{L} \frac{dx}{L}} = \frac{2}{L^3} \int_0^L xy dx \quad (11)$$

$$w_2 = \frac{\int_0^L xy dx}{\int_0^L x dx} = \frac{2}{L^2} \int_0^L xy dx \quad (12)$$

for the left ( $x < 0$ ) and right ( $x > 0$ ) side of the galaxy.

$w_1$  is dimensionless and proportional to the mean  $y/L$  displacement from the  $x$ -axis weighted by the distance from the center ( $x/L$ ), where  $L = \max(|x|)$ . The normalizing factor ( $1/L$ ) assures that  $w_1$  is independent of the choice of the measurement unit.  $w_2$  has units of kpc, and measures the average deviation from a horizontal plane of the galaxy weighted by  $x$  (horizontal axis). In each warp measure, the

error is calculated via standard propagation of the width of each column centroid.

We correct both warp measures for the inclination of the galaxy based on Geha et al. (2006). This is done by dividing the measured warp curve by  $\sin(i)$  where  $i = \sqrt{\frac{1-(b/a)^2}{1-0.19^2}}$  for a relative disk thickness of 0.19. The warp is estimated within three half-light radii of the galaxy (beyond this radius, the images tend to become very noisy), though the results of this section do not vary appreciably as this limit is changed from 2 to 4 half-light radii. In Appendix C4 we define a third warp measure, and show that the following results are unchanged.

## 5.2 Results

We classify the warp as ‘‘U-shaped’’ if  $w_1$  or  $w_2$  has opposite signs on the left and right sides, and ‘‘S-shaped’’ if the signs match. To quantify the warp strength, we average the absolute values of the warp in the left and right sides of the galaxy. Figure 8 shows the normalized distribution of  $w_1$  (left panel) and  $w_2$  (right panel) for screened and unscreened galaxies displaying a U-shaped warp. The errors in the histograms are estimated using Poisson statistics in each bin.

It is expected within modified gravity that unscreened galaxies with close neighbors will preferentially show large U-shaped warps. A K-S test shows that the  $w_1$  distributions are similar between the screened and unscreened samples: this implies that the appearance of warp does not depend on the screening level. However, we find that  $w_2$  distributions are marginally different: the unscreened galaxies are slightly more warped. The null hypothesis that the screened and unscreened distributions are identical is accepted only with a probability  $\sim 0.88$ . In Appendix C1 we show that this difference can be attributed to size or distance bias. In Appendix C4 we show that warp distributions remain similar even if we expand the sample to include all types of observed warps.

The distance-dependent effect, described in Appendix

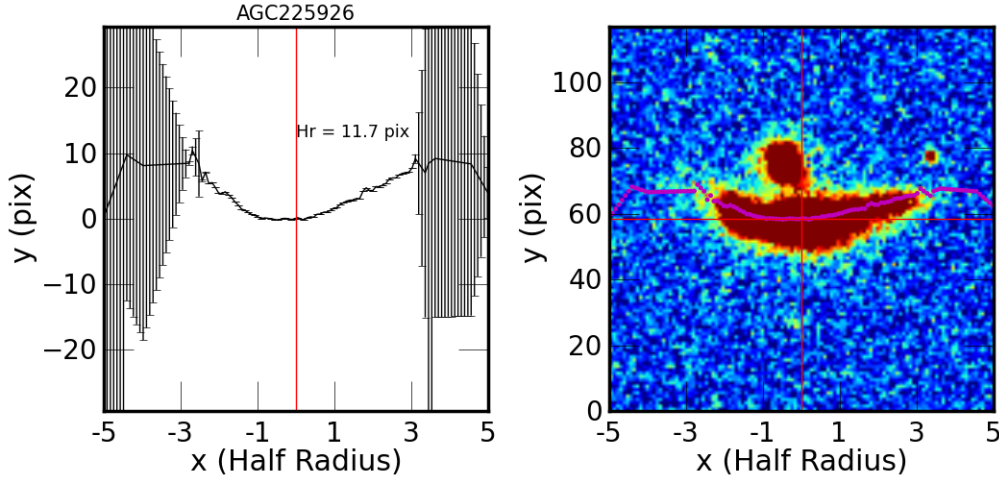


**Figure 7.** An example of the estimation of warping from a disk galaxy image. The left panel shows the estimated warp curve. The red vertical line shows the  $x$ -center of the galaxy. The  $x$ -axis is given in the unit of half light radius ( $h_r$ ) of the galaxy. In the right panel we superimpose the warp curve on the optical image of the galaxy.

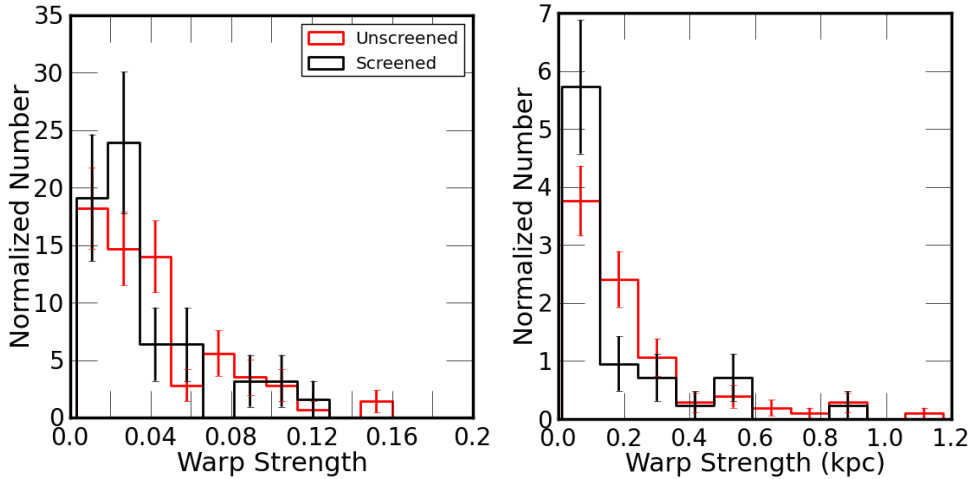


**Figure 8.** The distribution of warps for screened and unscreened galaxies for  $f_{R0} = 2 \times 10^{-7}$ . The left panel shows the dimensionless warp estimated using Eq.11 and the right panel shows the estimate in kpc using Eq.12. No significant difference is found between the distributions of warps of screened and unscreened galaxies in the left panel. A marginal difference is found on the right with more warp for unscreened galaxies. This discrepancy does not remain if we account for size bias as discussed in the text.

C1, suggests that the ideal way to compare the  $w_2$  of screened and unscreened samples is to consider only galaxies of similar physical size. The left panel of Figure 9 shows the warp  $w_2$  versus the half light radius of galaxies. As expected, the warp is larger for bigger galaxies. Small points indicate measured values, and the large points show the average and dispersion within 0.5kpc bins in half-light radius (see Appendix A). The lines shows the best fit linear relation between the half light radius and the warp, with slopes listed in the top left corner. We see that when comparing galaxies of similar size, the warp is equivalent: this indicates that the difference of distributions in the right panel of 8 is due to this size bias.

### 5.3 Comparison with theory

Our analysis of galaxy warp shows that there exists no significant difference between the occurrence of warps in screened and unscreened samples. Here we use this non-detection to place limits on strength of the fifth force. Given the low levels of observed warps, we assume that any contribution due to modified gravity will be added linearly to astrophysical effects which are estimated from the screened sample: under this assumption, to determine the warp associated with MG, we subtract the screened value from the unscreened value.

We find the average warp ( $\langle w_1 \rangle$ ) and error on the average using the method described in Appendix A. We find that  $\langle w_1 \rangle = 0.035 \pm 0.014$  for unscreened galaxies and  $\langle w_1 \rangle = 0.032 \pm 0.020$  for screened galaxies (i.e. the warp due to astrophysical process is a 3% effect) for  $f_{R0} = 2 \times 10^{-7}$ .

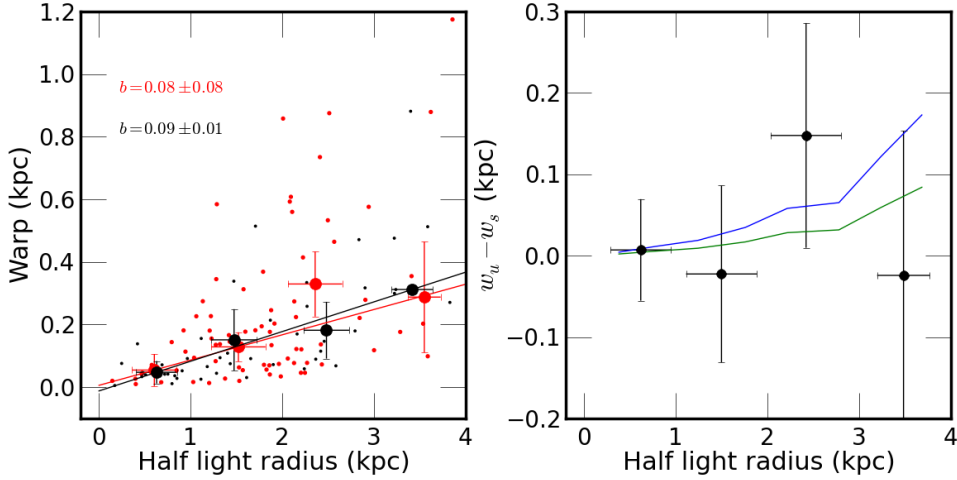


**Figure 9.** The left panel shows the strength of the warp in kpc as a function of galaxy size. The small black and red dots represent individual measurements of screened and unscreened galaxies for  $f_{R0} = 2 \times 10^{-7}$ . The large circles with error bars show the average warp. The lines are the best fit linear relation to these averages. The slopes of the lines are shown in the top left corner. The right panel shows the estimated contribution to the warp due to MG, i.e., the difference between warp of unscreened ( $w_u$ ) and screened samples ( $w_s$ ). The blue and green lines shows the predictions with  $\Delta G/G = 1$  and  $\Delta G/G = 1/3$ . Given the error bars, we are unable to test these models.

This implies that the estimated warp in a modified gravity scenario ( $\hat{w}_{MG}$ ) is as low as  $0.003 \pm 0.024$  (0.3%). See Table C1 for the results of other background field values. We can use this in conjunction with a theoretical expectation of the warp strength to place loose constraints on modified gravity. This expected warp can be estimated as described by Jain & Vanderplas (2011); the result is sensitive to the mass profile of the galaxy, as well as the strength of the external potential gradient. Unfortunately, both these are difficult to determine from the data.

To estimate the external potential gradient, we follow Jain & Vanderplas (2011) and assume that a galaxy will acquire a velocity of  $\sim 100$  km/s in 3 Gyr. This gives an average acceleration of  $\sim 10^{-15}$  km/s<sup>2</sup>. We also need to consider the direction of this force at the galaxy to get the effective force to generate the warp. We marginalize over the angle by averaging 1000 random angles between -90 deg and 90 deg. The mass at a given radius of the galaxy is found by the assumption of cored isothermal sphere. Based on these assumptions we generate warp curves for these galaxies. This analysis leads to a theoretical prediction of the modified gravity warp contribution of  $w_{MG} = 0.003^{+0.003}_{-0.001}$  ( $w_{MG} = 0.006^{+0.006}_{-0.003}$ ) for  $\Delta G/G = 1/3$  ( $\Delta G/G = 1$ ), with errors indicating the scatter in predicted values.

The right panel of Figure 9 shows the average values of  $w_2$ , as well as the theoretical predictions outlined above, as a function of galaxy size (these values are tabulated in Table C1). The blue and green lines show the expected warp for  $\Delta G/G = 1$  and  $1/3$ , respectively. The large error in the measured values is due primarily to the fact that we are looking for a relatively small effect in a small sample of galaxies. The figure indicates that the measured warp is not precise enough to distinguish between modified gravity and GR, which corresponds to zero warp in this figure.

#### 5.4 Future Directions

Our study of galaxy warps cannot rule-out either the predictions of MG or of GR. The two limitations are the relative scarcity of objects with kinematic data (like ALFALFA), and the uncertainty in halo parameters that goes into the warp prediction.

Based on our estimates of uncertainties in the measured and predicted warps we can estimate the number of galaxies with kinematic data required to reduce the error in the observed warp by a factor of 8 (so that the measurement error is comparable to the uncertainty in the predictions). We need  $\sim 8,000$  dwarf galaxies to test  $f_{R0} = 2 \times 10^{-7}$  and  $\sim 20,000$  galaxies for  $f_{R0} = 1 \times 10^{-6}$  (calculated from third and fourth lines of Table C1). This assumes that the halo parameters have the same accuracy as we have in this paper. Note also that even though the number of galaxies required to test  $f_{R0} = 2 \times 10^{-7}$  is a factor of two less than that of  $f_{R0} = 1 \times 10^{-6}$ , those galaxies should be very low mass and isolated, and therefore will require deep surveys. Another avenue of improvement is to obtain better optical images from current surveys (e.g Dark Energy Survey). This imaging should be supplemented by spectroscopic or 21cm surveys which can measure rotation velocities.

## 6 STELLAR AND GASEOUS VELOCITY ROTATION CURVES

In this section we explore the use of kinematic measures to detect effects of modified gravity. There are two classes of expected effects, both predicted by Jain & Vanderplas (2011). First, in the presence of a background potential gradient, a galaxy with a rotation axis perpendicular to the gradient will exhibit a distorted stellar rotation curve. Second, within the galaxy, the unscreened material will feel a stronger force and thus have its rotation curve enhanced by a

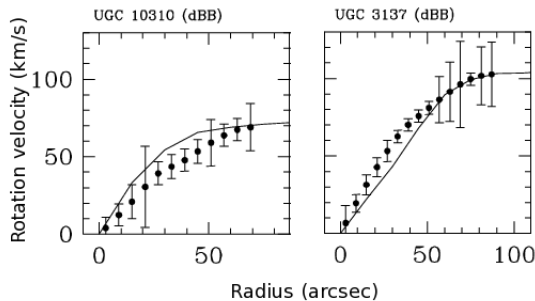


**Figure 10.** An example of rotation curves for two galaxies, measured in  $H\alpha$  (dots with error bars) and HI (solid lines). The data are taken from Swaters et al. (2009).

factor of  $\sqrt{1 + \Delta G/G}$ . Both these measures depend on finding an accurate tracer of the kinematics of main sequence stars. We discussed  $H\alpha$  as a potential tracer in Section 3.2; we return to this subject here before proceeding with one of these tests.

### 6.1 HI- $H\alpha$ velocity difference

Historically,  $H\alpha$  emission has been assumed to trace the stellar rotation curve. Because it originates in HII regions near hot stars, this assumption is well founded. However, as we argued in Section 3.2, this assumption may not hold in a modified gravity scenario. Because of the potentially complicated dynamical scenario of stars which lag behind the HII regions they create, however, simple arguments such as these may be incomplete.

In this section, we address this question empirically by comparing the  $H\alpha$  rotation curve to that of HI, which is associated with unscreened gaseous component. Any similarity between these two within unscreened galaxies would indicate the safety of our assumption that  $H\alpha$  emission traces the unscreened galaxy component.

In order to estimate the difference between HI and  $H\alpha$  rotation curves, we extract HI and  $H\alpha$  data from Figure 3 of Swaters et al. (2009), which contains 22 galaxies. The errors in  $v_{HI}$  were obtained by private communication with Swaters. Each HI observation has one or two  $H\alpha$  counterparts (see the references therein); in addition, we have  $H\alpha$  data for 14 galaxies from GHASP. Note that all galaxies in the sample can safely be assumed to be unscreened due to their low mass and lack of massive neighbors. In Figure 10 we show the comparison of HI and  $H\alpha$  rotation curves for two galaxies taken from Swaters et al. (2009): the galaxy in the left panel has  $HI > H\alpha$ , while the galaxy in the right panel has  $HI < H\alpha$ .

To quantify the difference between HI and  $H\alpha$  rotation curves statistically we first average both sides of the HI and  $H\alpha$  rotation curves separately about a common center to reduce the observational uncertainty in the measured rotation curves, and then compare the HI and  $H\alpha$  curves to estimate the weighted average velocity difference,  $\Delta v = v_{HI} - v_{H\alpha}$ . If both  $H\alpha$  and HI rotate similarly, then the  $\Delta v$  will be approximately normally distributed about zero. In Figure 11 we plot the distribution of  $v_{HI} - v_{H\alpha}$  in black for Swaters

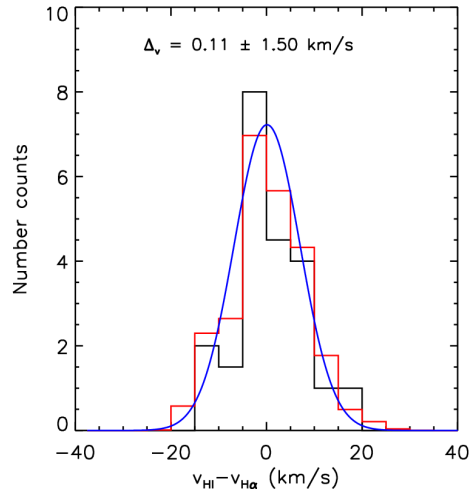


**Figure 11.** The difference between HI and  $H\alpha$  rotation velocities. We plot the distribution of  $\Delta v = v_{HI} - v_{H\alpha}$  for the Swaters et al. (2009) data (black histogram). The red histogram includes individual errors in the  $\Delta v$  measurements. We over plot in blue the best fit Gaussian. The mean value of the difference is indicated as well, showing that the rotation curves agree to better than 2 km/s.

et al. (2009) data. When more than one  $H\alpha$  measurement is provided for the same galaxy, we weight equally the contribution of each  $\Delta v$  to the mean. Accounting for errors in the observed values gives the red histogram.<sup>4</sup> The best-fit Gaussian is indicated by the blue curve.

We obtain  $\langle \Delta v \rangle = 0.11 \pm 1.50 \pm 5$  km/s (statistical and systematic error) when we use HI and  $H\alpha$  from Figure 3 of Swaters et al. (2009). Combining different  $H\alpha$  observations and testing different ranges in the velocity curve leads to a 2 km/s contribution to the systematic error; the remaining 3 km/s comes from the potential for asymmetric drift & non-circular motion to affect the relationship (Swaters et al. 2009; de Blok & Bosma 2002). The errors additionally include those due to both measurement and non-circular motions, which we found by taking the difference between approaching and receding sides. See Swaters et al. (2009) for details.

With these affects accounted for, we find that the HI and  $H\alpha$  rotation curves are consistent. This consistency confirms that it is safe to assume that  $H\alpha$  traces the unscreened, gaseous component of the galaxy even in the presence of a fifth force.

### 6.2 Asymmetry in $H\alpha$ rotation curves

In the previous section, we show that if MG is true, then  $H\alpha$  empirically traces the unscreened gaseous component of the galaxy. This implies that the  $H\alpha$  rotation curve will be nearly symmetric about the center of dark matter halo. On the other hand, the dark matter halo will be offset from

<sup>4</sup> In order to take into account individual errors and intrinsic dispersion to calculate the mean and the error we follow the procedure described in Appendix A.

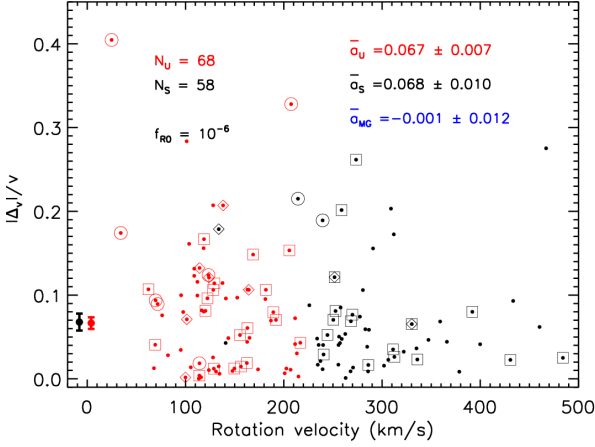


**Figure 12.** The  $H\alpha$  rotation curve asymmetry  $a = |\Delta v|/v$  is shown as a function of rotation velocity for galaxies from the GHASP survey. Black (red) points indicate screened (unscreened) galaxies for  $f_{R0} = 10^{-6}$ . The mean and standard deviations of each distribution are shown by the large dots at the left of the plot. The shapes of individual points indicate the morphology of the rotation curves: diamonds indicate smoothly asymmetric curves, squares indicate barred galaxies, and empty circles indicate irregular galaxies. See text for details.

the stellar component and therefore the  $H\alpha$  curve will be asymmetric with respect to the optical centroid, with an asymmetry on the order of 10-15 km/s. We note that this asymmetry is a manifestation of the offset between the stellar and dark matter halo, and is distinct from the stellar rotation curve asymmetry predicted by Jain & Vanderplas (2011).

In this section we use  $H\alpha$  rotation curves to test whether gaseous rotation curves are asymmetric about the stellar centroid, by comparing the approaching and receding sides of the  $H\alpha$  rotation curves about the associated stellar centroid. Any positive signal may indicate the presence of fifth force.

### 6.2.1 Data and visual classification of rotation curves

We use  $H\alpha$  rotation curves for nearly 200 disk galaxies from the Gassendi  $H\alpha$  survey of spirals (GHASP) archive (see Epinat et al. 2008, and references therein) to search for asymmetry in rotation curves. GHASP is an  $H\alpha$  kinematic survey of spiral and irregular galaxies. This survey has observed  $\sim 220$  galaxies, and provides the rotation curves for both approaching and receding sides separately. We correct the velocities for inclination by assuming thin circular disk.

We visually inspect these rotation curves and classify them into symmetric, smoothly asymmetric and irregular. We show a sample of symmetric curves in Figure D3 and smoothly asymmetric in Figure D4 in Appendix D. In a modified gravity scenario, we expect the gaseous rotation curves to be smoothly asymmetric about the stellar centroid (Jain & Vanderplas 2011). We remove all the irregular rotation curves which have too few observed points and/or small-scale discontinuities: these are primarily associated with small, dim and/or morphologically irregular

galaxies, and the rotation curve shapes are more likely due to small-scale astrophysical effects than to a fifth-force type effect. We find that in both the screened and unscreened sample, symmetric curves outnumber smoothly asymmetric curves by a factor of four. We emphasize, however, that the galaxies with asymmetric  $H\alpha$  curves may be ideal for a future systematic search for the dynamical effects of modified gravity.

### 6.2.2 Analysis

We quantify the asymmetry in rotation curves for each galaxy using the absolute value of the weighted average of difference between approaching and receding sides of the rotation curves ( $|\Delta v|$ ) about the stellar centroids (Epinat et al. 2008). This asymmetry is better seen near the center of the galaxy and therefore we focus on the inner part of the rotation curves. However, we find that our results do not depend significantly on the location of the measurement. Finally, we define the asymmetry coefficient  $a \equiv |\Delta v|/|v_{max}|$  where  $v_{max}$  is the maximum rotation velocity, since we expect any asymmetries to scale with galaxy mass. The error in the asymmetry includes both measurement error and intrinsic dispersion  $\sigma_a$ , which can be same order of magnitude; we follow the method described in Appendix A. In a similar manner as the previous sections, we assume that the asymmetry of unscreened galaxy,  $a^U$  is a linear combination of  $a^{MG}$ , the modified gravity contribution, and  $a^X$ , the contribution from standard astrophysical forces.

### 6.2.3 Results

We summarize the results in Figure 12. We plot  $a$  as a function of maximum rotation velocity of the galaxies for  $f_{R0} = 10^{-6}$ . There are 68 unscreened galaxies (shown in red) and 58 screened galaxies (shown in black). We compute the asymmetry within the central region of the rotation curve, up to 30% the optical radius of the galaxy.

The shapes of the individual symbols indicate the visually-determined galaxy morphology: the diamond symbols indicate galaxies with visual asymmetry in the rotation curve which look interesting under modified gravity theories. Square symbols indicate barred galaxies and empty circles represent irregular cases. There is no clear correlation between these morphologies and the measured asymmetry. The filled points on the left of the plot show the mean and standard deviation of the asymmetries for the screened and unscreened components. We find that the asymmetry for both screened and unscreened galaxies is around 7% which corresponds to asymmetries in the range of 10-20 km/s. Subtracting these mean values implies an asymmetry produced by modified gravity of  $a^{MG} = -0.001 \pm 0.012$ . If we instead assume  $f_{R0} = 10^{-6.5}$  (24 unscreened galaxies and 102 screened galaxies) we find  $a^{MG} = 0.024 \pm 0.015$ . In either case, a 10% asymmetry predicted for modified gravity can be ruled out at approximately the 5- $\sigma$  level.

Note that these results do not attempt to correct for asymmetric drift or non-circular motion. We have further analyzed this data and found no correlation between asymmetry and the number of neighbors or distance to the nearest neighbor, which would be present if the asymmetries

were caused by a fifth force. Garrido et al. (2005) also studied asymmetry in GHASP H $\alpha$  rotational curves. They conclude that both isolated and softly interacting galaxies have similar level of asymmetry, which might be due to inhomogeneous massive star formation regions.

## 7 DISCUSSION AND CONCLUSIONS

We have explored several astrophysical tests of modified gravity which rely on partially-screened dwarf galaxies in which fifth force effects act on diffuse components (gas, dark matter, and giant stars), while more compact components (main sequence stars) are screened from these effects. These tests probe regions of the parameter space of chameleon type gravity theories which have not been probed by cosmological tests or laboratory experiments. The observables include offsets between the stellar and gaseous components, warping of stellar disks, and asymmetry in the gaseous rotation curves. Our study relies on a variety of previously-published observational data.

### 7.1 Summary of results

- *Offset between HI gas and stars:* The offset study based on optical and HI gas centroids shows that it is not possible to distinguish between gravity theories using the current HI data. The accuracy of the astrometry is principally limited by the large beam size of the 21cm observations. However, with a larger catalog of candidate galaxies and/or more accurate radio astrometry, this test may provide competitive constraints in the future. In this section we summarize our results, discuss systematic errors and examine prospects for improved tests.

- *Offset between optical and dynamical center:* An alternative means of measuring this expected offset, the difference between the optical centroid and the kinematical centroid of H $\alpha$ , is much more precise and limits the component of modified gravity scatter to  $\sim 2\%$  of the optical radius of the galaxy, ruling out 5% scatter at the  $3\text{-}\sigma$  level.

- *Offset between red giants and main sequence stars:* We show that the offset between the partially-screened red giant population and the fully-screened main sequence population is too sensitive by systematic effects to provide any meaningful power to distinguish between gravity theories: the data is consistent with both GR and MG at a  $2\text{-}\sigma$  level. This test has the potential to improve as more stellar populations are observed within nearby dwarf galaxies.

- *Warps in edge-on galaxies:* The warp study relies on measurements of the optical morphology of stellar disks of late-type galaxies observed by SDSS. We find that the warp measures for this galaxy sample are consistent with both GR and modified gravity theories: the main limitation is the relatively small number of suitable galaxies for which kinematic data is available in order to estimate the screening level of the galaxies in the sample.

- *Rotation curve tests:* In the final test we used the GHASP galaxy sample to estimate the asymmetry in the H $\alpha$  rotation curves, which arises due to the offset between the screened stellar component and the unscreened gaseous component. We find that the asymmetry attributable to modified gravity is as low as  $(-0.1 \pm 1)\%$ , compared to the

expected value of 10% under favorable conditions. This implies that the modified gravity models which predicts 10% asymmetry can be rule out at  $5\sigma$  level. However, this test carries two major uncertainties: systematic uncertainties in the data due to effects of asymmetric drift and non-circular motions, and systematic uncertainties in the theoretical expectation due to insufficient knowledge of the internal halo parameters and external environment of each galaxy.

Finally, we examined individual rotation curves from the GHASP galaxy sample and classified them based on the different signatures in the curves (see Appendix D). We found that the majority of these galaxies have fairly symmetric curves regardless of their local density/potential. However, we identified a few galaxies with interesting features in the rotation curves. Some of these galaxies have other potential fifth force effects like U-type warps and optical offset from that of HI. More detailed studies of these individual cases can shed light on whether the features may be attributable to fifth-force effects or more traditional astrophysical processes.

### 7.2 Systematic errors and caveats

The tests performed here involve aggregate statistical comparisons between the unscreened galaxy sample and the screened (control) sample. One of the major assumptions in this type of study is that, apart from screening level, the two samples are statistically similar. As noted above, for many of the tests this division correlates with galaxy size. In some cases we attempt to minimize any potential bias by looking only at galaxies near the self-screening threshold (at the cost of weakening the signal). However, a more precise result could be obtained given a large sample of low-mass, environmentally screened galaxies. Galaxies in the two samples would then have the same distribution in size and mass. So we recommend that future studies in this direction prioritize new observations of low-mass galaxies in both the field and near large neighbors.

Another important caveat is that we use a large, heterogeneous data set to perform the above tests. Because the data were gathered without this type of test in mind, there was little specific attempt to control systematic errors that can affect explorations of modified gravity. One extreme example of this is the constraint based on separation of HI and optical centroids: the strength of the test is sensitive to the characteristics of the error in centroid determination: even a 10% overestimate of the error can impact the resulting constraints. Observing campaigns specifically designed for this sort of modified gravity test could yield homogeneous data sets with such systematic effects minimized.

The third major caveat comes from uncertainties in our estimate of the external potential at the locations of dwarf galaxies. We have estimated the Newtonian potential as well as the fifth force, estimated using the masses and locations of neighboring galaxies. This estimate is subject to the uncertainties in mass estimation of galaxies. It can be improved in a number of ways: completeness over the neighborhood of the dwarf galaxy sample, mass estimates using spectroscopic or 21cm observations, and better modeling of the mass and scalar field distribution. The improved modeling can be done by explicitly solving for the scalar field at each location, in-

cluding the presence of underdense regions that also contribute to the fifth force. For some of the tests only a  $\sim 10$  Mpc sized region needs to be studied in detail, so the observations and modeling are tractable.

### 7.3 Future prospects

Here we discuss specific ways to sharpen each of the tests we have carried out and summarized above in subsection 7.1. Before we get to these tests, we note that a variety of experiments can be used to test gravity theories, ranging from laboratory to cosmological scales. For chameleon type scalar-tensor theories, the first in our series of papers (Jain et al. 2012) used cepheid variable stars and other distance indicators to place stringent limits on the two parameters of the theories: the coupling  $\alpha$  (related to  $\Delta G/G$  in this paper) and the background field value (equivalent to  $f_{R0}$  in this paper). The upper limit for  $f(R)$  models obtained using cepheids correspond to  $\Delta G/G \simeq 1/3$ ;  $f_{R0} \simeq 5 \times 10^{-7}$ , or a fifth force range below 1 Mpc at cosmic mean density: these are far more stringent than limits from large-scale, cosmological tests as discussed by Jain et al. (2012). For tests using other tracers in the Milky Way, see Brax & Davis (2013) and reference therein.

Dwarf galaxy tests currently probe larger coupling values. However the field values probed can be lower, especially with the fainter dwarf galaxies within  $\sim 10$  Mpc of the Milky Way. The limits on both parameters can be improved significantly for all the tests we have considered. A brief account for each test follows, though detailed studies are needed to plan future observations.

- *Offset between HI gas and stars:* For this test to produce competitive constraints, it is crucial to improve the precision of the centroid measurement, either through telescopes with a smaller beam size, or through the stacking of many more galaxy images. Using the ALFALFA data, the error in the offset estimate is  $\sim 1$  kpc; to get an error of 100 pc we need to stack  $\sim 10^4$  galaxies. Furthermore, the characteristics of the error in the centroid must be understood at the few percent level. A better way forward would be to get improved resolution radio maps (e.g. via VLA observations), which would then relax the required sample size and lower the systematic uncertainty.

- *Offset between optical and dynamical center:* increasing the number of H $\alpha$  rotation curves to a few hundred low-mass galaxies would be sufficient to reduce the uncertainty of this measurement. More important is sophisticated modeling of the environment of each galaxy to determine screening levels and the strength of the expected signal.

- *Offset between red giants and main sequence stars:* Currently, the red giant displacement test is dominated primarily by systematic uncertainties. As the signal in this test is weaker than the other probes, the best approach would be to focus on a limited number of galaxies with a very well known external force (i.e. well-observed and well-modeled local environment). The uncertainty in the external force is the limiting factor if one wants to constrain modified gravity. Another potential approach would be to use integral-field galaxy spectra and estimate the contributions of red giant and main sequence populations as a function of location in the galaxy. A difference in these centroids could be

attributed to modified gravity, using control tests similar to those in this paper. This test is applied to a small number of very small but nearby galaxies (closer than 10 Mpc), so detailed studies of individual galaxies are feasible.

- *Warps in edge-on galaxies:* To reduce the observed error in the warp measurements to the level of uncertainty in the predicted values requires high-quality images of about 10,000 dwarf galaxies in very low density environments and 20,000 dwarf galaxies in low to moderately dense environments for  $f(R)$  theories with  $f_{R0} = 2 \times 10^{-7}$  and  $f_{R0} = 1 \times 10^{-6}$ , respectively. These numbers are feasible with current and ongoing galaxy surveys. With this increase in data, however, the limiting factor will be the knowledge of the distribution of halo parameters within galaxies of this size: the predicted strength of the observed warp is highly dependent on this mass profile. Rotation curves that extend to the inner parts of the disk can constrain the mass profile.

- *Rotation curve tests:* We have examined asymmetries in rotation curve data. In addition, a direct measurement of  $\Delta G/G$  can be made by comparing HI rotation curves with stellar rotation curves (section 3.1). However the stellar rotation curve must be measured using stellar absorption lines which arise very close to the surface of dwarf stars (not via H $\alpha$  as is common practice; see discussion in section 3.2). These curves are difficult to observe: depending on brightness, each galaxy may require several hours of observations with large telescopes. This test has the advantage that it does not depend on a detailed dynamical model or on the precise characteristics of the environment of the unscreened galaxy: for this reason, high-precision observations of a handful of the unscreened galaxies can lead to strong constraints on modified gravity theories, free of many of the systematic uncertainties discussed above.

## 8 ACKNOWLEDGMENTS

We are grateful to Xiaohu Yang and collaborators for providing us their SDSS group catalog and to Richard Swaters for rotation curve data. We have used published data from a variety of sources cited in the text. We thank Mike Jarvis for several valuable suggestions and Gary Bernstein, Andy Connolly, Julianne Dalcanton, Lam Hui, Kazuya Koyama, Elisabeth Krause, Adam Lidz, Karen Masters, Masao Sako, Matt Walker and Gongbo Zhao for helpful discussions. This work was partially supported by NSF grant AST-0908027.

Funding for the SDSS and SDSS-II has been provided by the Alfred P. Sloan Foundation, the Participating Institutions, the National Science Foundation, the U.S. Department of Energy, the National Aeronautics and Space Administration, the Japanese Monbukagakusho, the Max Planck Society, and the Higher Education Funding Council for England. The SDSS Web Site is <http://www.sdss.org/>.

The SDSS is managed by the Astrophysical Research Consortium for the Participating Institutions. The Participating Institutions are the American Museum of Natural History, Astrophysical Institute Potsdam, University of Basel, University of Cambridge, Case Western Reserve University, University of Chicago, Drexel University, Fermilab, the Institute for Advanced Study, the Japan Participation Group, Johns Hopkins University, the Joint Institute for Nuclear Astrophysics, the Kavli Institute for Particle As-



trophysics and Cosmology, the Korean Scientist Group, the Chinese Academy of Sciences (LAMOST), Los Alamos National Laboratory, the Max-Planck-Institute for Astronomy (MPIA), the Max-Planck-Institute for Astrophysics (MPA), New Mexico State University, Ohio State University, University of Pittsburgh, University of Portsmouth, Princeton University, the United States Naval Observatory, and the University of Washington.

## REFERENCES

- Abazajian K. N., Adelman-McCarthy J. K., Agüeros M. A., Allam S. S., Allende Prieto C., An D., Anderson K. S. J., Anderson S. F., Annis J., Bahcall N. A., et al. 2009, *ApJS*, 182, 543
- Abell G. O., Corwin Jr. H. G., Olowin R. P., 1989, *ApJS*, 70, 1
- Begum A., Chengalur J. N., Karachentsev I. D., Kaisin S. S., Sharina M. E., 2006, *MNRAS*, 365, 1220
- Begum A., Chengalur J. N., Karachentsev I. D., Sharina M. E., Kaisin S. S., 2008, *MNRAS*, 386, 1667
- Bertin E., Arnouts S., 1996, *A&AS*, 117, 393
- Brax P., Davis A.-C., 2013, *ArXiv e-prints*
- Brax P., van de Bruck C., Davis A.-C., Shaw D., 2010, *Phy. Rev. D*, 82, 063519
- Cabré A., Vikram V., Zhao G.-B., Jain B., Koyama K., 2012, *ArXiv e-prints*
- Chang P., Hui L., 2011, *ApJ*, 732, 25
- Dalcanton J. J., Williams B. F., Seth A. C., Dolphin A., Holtzman J., Rosema K., Skillman E. D., Cole A., Girardi L., Gogarten S. M., Karachentsev I. D., 2009, *ApJS*, 183, 67
- Davis A.-C., Lim E. A., Sakstein J., Shaw D. J., 2012, *Phy. Rev. D*, 85, 123006
- de Blok W. J. G., Bosma A., 2002, *A&A*, 385, 816
- Ebeling H., Voges W., Bohringer H., Edge A. C., Huchra J. P., Briel U. G., 1996, *MNRAS*, 281, 799
- Epinat B., Amram P., Marcelin M., Balkowski C., Daigle O., Hernandez O., Chemin L., Carignan C., Gach J.-L., Balard P., 2008, *MNRAS*, 388, 500
- Evrard A. E., Bialek J., Busha M., White M., Habib S., Heitmann K., Warren M., Rasia E., Tormen G., Moscardini L., Power C., Jenkins A. R., Gao L., Frenk C. S., Springel V., White S. D. M., Diemand J., 2008, *ApJ*, 672, 122
- Garrido O., Marcelin M., Amram P., Balkowski C., Gach J. L., Boulesteix J., 2005, *MNRAS*, 362, 127
- Geha M., Blanton M. R., Masjedi M., West A. A., 2006, *ApJ*, 653, 240
- Giovanelli R., Haynes M. P., Kent B. R., Perillat P., Saintonge A., Brosch N., Catinella B., Hoffman G. L., Stierwalt S., Spekkens K., Lerner M. S., Masters K. L., 2005, *AJ*, 130, 2598
- Giovanelli R., Haynes M. P., Kent B. R., Saintonge A., Stierwalt S., Altaf A., Balonek T., Brosch N., Brown S., Catinella B., Furniss A., Goldstein J., 2007, *AJ*, 133, 2569
- Hinterbichler K., Khoury J., 2010, *Physical Review Letters*, 104, 231301
- Hu W., Sawicki I., 2007, *Phy. Rev. D*, 76, 064004
- Hui L., Nicolis A., 2010, *Physical Review Letters*, 105, 231101
- Hui L., Nicolis A., Stubbs C. W., 2009, *Phy. Rev. D*, 80, 104002
- Jain B., 2011, *Royal Society of London Philosophical Transactions Series A*, 369, 5081
- Jain B., Khoury J., 2010, *Annals of Physics*, 325, 1479
- Jain B., Vanderplas J., 2011, *ArXiv e-prints*
- Jain B., Vikram V., Sakstein J., 2012, *ArXiv e-prints*
- Jiménez-Vicente J., Porcel C., Sánchez-Saavedra M. L., Battaner E., 1997, *Ap&SS*, 253, 225
- Karachentsev I. D., Karachentseva V. E., Huchtmeier W. K., Makarov D. I., 2004, *AJ*, 127, 2031
- Kent B. R., Giovanelli R., Haynes M. P., Martin A. M., Saintonge A., Stierwalt S., Balonek T. J., Brosch N., Koopmann R. A., 2008, *AJ*, 136, 713
- Khoury J., Weltman A., 2004, *Phy. Rev. D*, 69, 044026
- Lavaux G., Hudson M. J., 2011, *MNRAS*, 416, 2840
- Martin A. M., Giovanelli R., Haynes M. P., Saintonge A., Hoffman G. L., Kent B. R., Stierwalt S., 2009, *ApJS*, 183, 214
- Mathewson D. S., Ford V. L., Buchhorn M., 1992, *ApJS*, 81, 413
- Persic M., Salucci P., 1995, *ApJS*, 99, 501
- Reiprich T. H., Böhringer H., 2002, *ApJ*, 567, 716
- Saintonge A., Giovanelli R., Haynes M. P., Hoffman G. L., Kent B. R., Martin A. M., Stierwalt S., Brosch N., 2008, *AJ*, 135, 588
- Schmidt F., Vikhlinin A., Hu W., 2009, *Phy. Rev. D*, 80, 083505
- Swaters R. A., Madore B. F., van den Bosch F. C., Balcells M., 2003, *ApJ*, 583, 732
- Swaters R. A., Sancisi R., van Albada T. S., van der Hulst J. M., 2009, *A&A*, 493, 871
- Swaters R. A., Sancisi R., van Albada T. S., van der Hulst J. M., 2011, *ApJ*, 729, 118
- Swaters R. A., van Albada T. S., van der Hulst J. M., Sancisi R., 2002, *A&A*, 390, 829
- Tully R. B., Fouque P., 1985, *ApJS*, 58, 67
- Will C. M., 2006, *Living Reviews in Relativity*, 9, 3
- Yang X., Mo H. J., van den Bosch F. C., Pasquali A., Li C., Barden M., 2007, *ApJ*, 671, 153

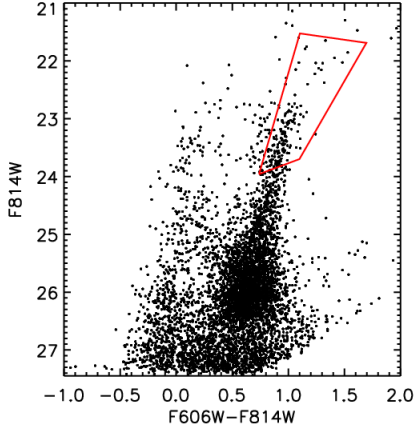


**Figure B1.** Color-magnitude diagram for galaxy DDO187, using filters F606W and F814W. The red region shows the selected red giants, that reside at the bright tip of the red giant branch.

## APPENDIX A: ALGORITHM TO FIND INTRINSIC DISPERSION

In most of the probes that we consider in this paper, there is an intrinsic dispersion associated with the estimated parameter due to astrophysical systematic effects that can be larger than the error in individual measurements. Because we weight the data by the inverse variance while calculating the mean value, including an intrinsic dispersion keeps data points with small measurement errors from being inappropriately over-weighted. It leads to an improved estimate of the mean and the error in the mean value. Here we describe our approximate procedure to estimate the intrinsic dispersion, and the improved mean and the error in the mean.

We have set of  $N$  observed values  $x_i$  and errors  $\sigma_i$ . We calculate the weighted average as

$$\bar{x} = \frac{\sum_i x_i w_i}{\sum_i w_i} \quad (\text{A1})$$

where  $w_i = 1/\sigma_i^2$ . Now, we add a constant systematic error  $\sigma_s$  to all the individual errors as  $\sigma_{\text{eff},i}^2 = \sigma_i^2 + \sigma_s^2$  which accounts for the intrinsic dispersion. For a Gaussian random variable this satisfies:

$$\sum_i \frac{(x_i - \bar{x})^2}{\sigma_{\text{eff},i}^2} = N \quad (\text{A2})$$

Now we recalculate the mean  $\bar{x}$  using Eq. A1 with  $w_i = 1/\sigma_{\text{eff},i}^2$ . This process continues until it converges. Finally, the error on the average  $\bar{x}$  will be calculated by

$$\sigma_{\bar{x}}^2 = \frac{1}{\sum_i 1/\sigma_{\text{eff},i}^2} \quad (\text{A3})$$

## APPENDIX B: RED GIANT STARS

In this section we summarise the potential systematic errors related to test based on red giant stars. In Figure B1 we show an example of color-magnitude diagram to illustrate the selection of red giant stars.

In the left panel of Figure B2 we explore whether the observed displacement between the red giant and main sequence populations is correlated with the distance to the galaxy. The data shows a small positive correlation between distance and displacement. To check whether this might affect the conclusions of Section 4.3, we divide the sample in different distance bins and reanalyze them in individual bins. We find that our conclusions do not change significantly even if we consider galaxies at similar distances.

In the right panel of Figure B2 we plot the correlation between the displacement and a measurement of asymmetry. The asymmetry is defined as the difference in centroids of main sequence stars at two different isocontours of stellar number density describing inner and outer part of the galaxy. We see that red giant displacement is strongly correlated with this asymmetry measurement, indicating that the effect may be related to the internal structure of the galaxy rather than being due entirely to a fifth-force effect. We note, however, that similar morphological asymmetry may occur in the presence of modified gravity as well. However, if we find the presence of similar effects in a screened galaxy sample then we will be able to separate the modified gravity effects from internal structure of the galaxy.

We also checked if the displacement is correlated with the number of stars (i.e. shot-noise), the ratio of red giants compared to the number of main sequence stars, the luminosity of the galaxy (indicative of mass and size), the HI line width (also indicator of mass), filters used to determine red giants or magnitude limit in the whole sample which depends on the camera used. None of these observables show appreciable correlation with the displacement of red giants.

We examined the effect of differences in the area that we used to calculate the centroid of main sequence stars and red giants. Usually the galaxy is not well centered in the image, that is the reason why we have to study systematics in the definition of the galaxy limiting area. Although it is easier to define isocontours in number counts using all the stars, there are a lot of interlopers (faint stars) that do not belong to the galaxy. We recalculated the centroid after gradually removing the faintest stars. We include galaxies only if their centroids converge after removing 20% of faintest stars. We also test if crowded regions can bias the result based on flags defined in Dalcanton et al. (2009). Due to longer exposure times, large number of faint foreground star will be detected which leads to poor photometry of individual stars. Moreover, we have calculated the centroid of main sequence stars weighting by luminosity, and still the displacement of red giants is consistent. Finally, we change our definition of red giants by going 0.5 magnitudes fainter, and we exclude bright stars from the definition of main sequence stars, and conclusions remain the same.

We also checked if the displacement is related to the number of stars (shot-noise), the ratio of red giants compared to the number of main sequence stars, the luminosity of the galaxy (indicative of mass and size), the HI line width (also indicator of mass), filters used to determine red giants or magnitude limit in the whole sample which depends on the camera used. None of these observables are correlated with the displacement of red giants.

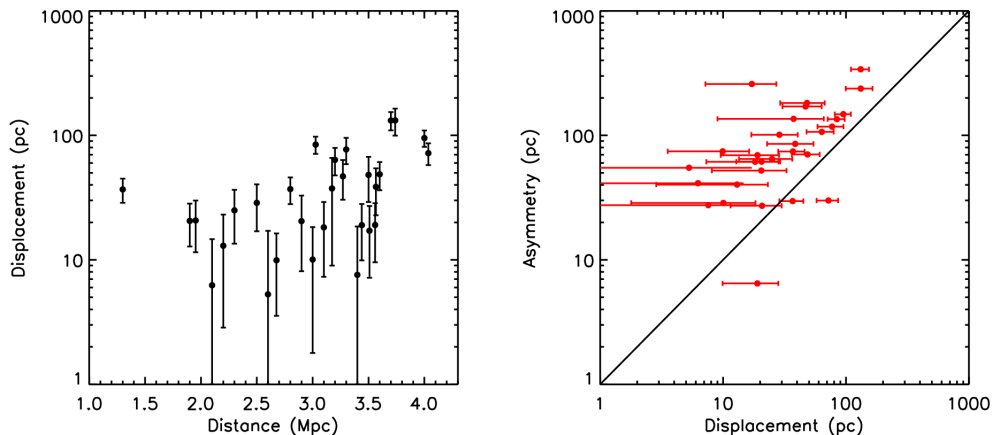


**Figure B2.** We plot distance vs displacement in the left panel to study systematic effects due to lower resolution for more distant galaxies. In the right panel, we plot the correlation between red giants displacement and degree of asymmetry of the galaxy (the straight line shows  $y=x$ ). Note how the asymmetry is bigger than the displacement in almost all the cases, suggesting that the displacement is just a result of internal structure.

## APPENDIX C: MEASUREMENT OF WARPS

In this section we describe the systematic effects related to the measurement of warps in section 5. We explore the bias due to distance effects, inclination effects, and environment. Finally, we propose a third warp estimator and show that the conclusions of Section 5 are unchanged.

### C1 Distance Bias

A number of systematic effects may be involved in the warp analysis. The first is bias related to distance. In our sample there exists a strong correlation between distance and average physical galaxy size: this is due to the fact that it is difficult to observe physically smaller galaxies at higher distances. If the measured warp depends on the size of the galaxy, then the comparison between screened and unscreened samples should be done as a function of distance to limit systematic effects due to the different samples. We check the distance bias by plotting the warp parameter against distance to the galaxies. The left panel of Figure C1 shows that the normalized warp parameter,  $w_1$ , is independent of the distance to the galaxy, as expected.

On the other hand, the estimator  $w_2$  does depend on the size of the galaxy: two galaxies with identical  $w_1$  curves will differ in  $w_2$ , depending on the size of the galaxy. Therefore, the size-distance relation implies that the estimated values of  $w_2$  will be higher at larger distances. The right panel of Figure C1 shows that this is indeed true. It should be noted that we have a systematically higher fraction of screened galaxies at smaller distance. We found that these galaxies belong to the Virgo cluster at distance  $\sim 17$  Mpc. Therefore, when we consider all the galaxies irrespective of their size, the screened sample has a smaller average value of  $w_2$  compared to that of unscreened galaxies due to the large fraction of screened galaxies at smaller distances. That is, the marginal difference between  $w_2$  distributions of screened and unscreened samples can be explained by this effect (compare figure 8 and Figure C1).

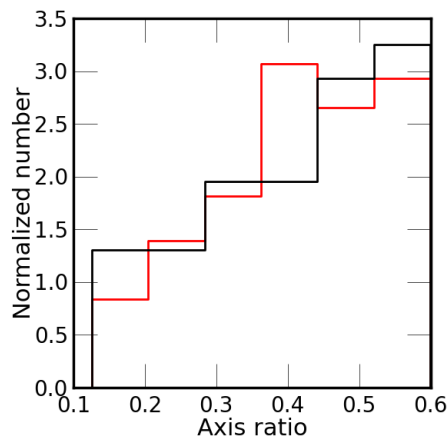


**Figure C2.** The distribution of axis ratio for screened and unscreened galaxies with  $f_{R0} = 2 \times 10^{-7}$ . We find no difference between the two samples.

### C2 Inclination Bias

Another potential systematic effect may be related to the inclination of the galaxy. While the warp can be well-estimated in edge-on galaxies, the apparent warp may be nearly zero for warped face-on galaxies. This is the source of the bias introduced by inclination. If the unscreened galaxies are systematically more inclined than the screened galaxies, then the warp parameter estimation will be more robust for unscreened galaxies. We therefore, check whether there is any systematic difference between the distributions of axis ratio for screened and unscreened galaxies. Figure C2 shows that the axis ratio of both screened and unscreened galaxies are distributed similarly. So we conclude that inclination affects the screened and unscreened galaxies equally, and therefore is unlikely to bias our result.

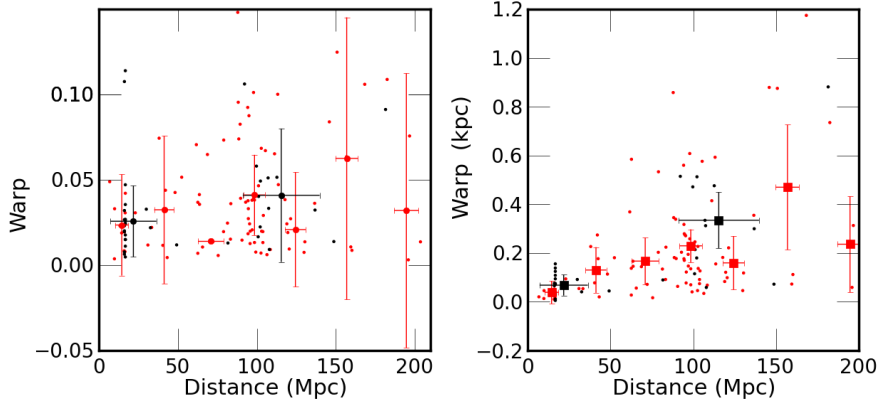


**Figure C1.** Systematic effects involved in the warp test. The left panel shows the warp ( $w_1$ ) vs distance (Eq. 11), right panel shows warp in kpc vs distance (Eq. 12) for screened and unscreened galaxies. If the screened sample is systematically closer than unscreened galaxies, then we measure a lower value of warp for screened sample compared to unscreened sample, which goes in the same direction as the modified gravity prediction.

### C3 Environmental Bias

An additional test we can perform with the data is to check whether there is any noticeable difference in the fraction of galaxies displaying U-shaped warps between the screened and unscreened samples. In the modified gravity scenario we expect that the fraction of U-shaped warps will be larger in the unscreened sample than in the screened sample. For this test we classify galaxies as U-shaped only if the galaxy has more than 3% warp, i.e. if  $w_1 > 0.03$ . As above, if the signs of left and right side warp are different then we classify them as U-type.

Figure C3 shows that the fraction of U-shaped warps does not depend on the screening level. This implies that any physical process which causes the formation of U-shaped warp works irrespective of the local density of the galaxy. It should be noted that this result does not vary with the choice of lower threshold value of the warp (i.e.  $w_1 > 3\%$ ) to define the U-warp. In the following section, we further show that the fraction of S-shaped warps is also consistent between the screened and unscreened sample.

### C4 Distribution of warps

In Section 5 we have shown that the distribution of U-type warp does not depend on the environment. However, we include only U-type warp in that analysis. Here we check whether the conclusion in section 5 still holds if we include all kind of warp in the analysis. For this purpose we define the *effective* total warp ( $w_e$ ) of galaxies as the absolute value of the difference between the warp of left and right hand sides of the galaxy. As we explained before the U-type galaxies will have opposite signs for left and right side warps and S-type/N-type will have same signs for both sides. Therefore, our definition of  $w_e$  will lead to larger value for a symmetric U-type warp and zero for other cases. However, the other type of warps can also give smaller non-zero values for  $w_e$  depending on the asymmetry of the warp curve. The same applies to U-type warp where the  $w_e$  can be smaller for weak warp curves. We find that almost all galaxies, except U-type warps, have  $w_e < 0.1$  with warp

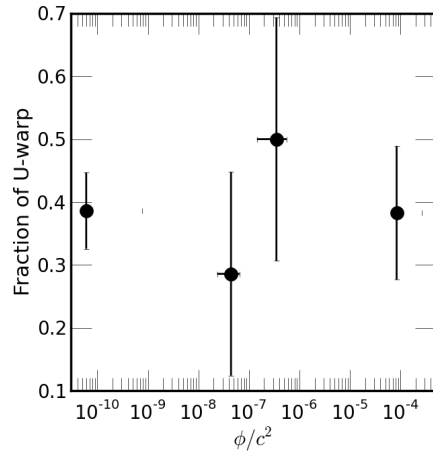


**Figure C3.** The fraction of galaxies displaying U-shaped warps vs the magnitude of the external potential. In this plot, galaxies are classified as U-shaped only if the warp is greater than or equal to 3%.

definition Eq 11. It is shown in the left panel of Figure C4. Also, we found that the distribution of  $w_e$  does not have any dependence on the environment and it is shown in the middle panel of Figure C4. We also found that there is no noticeable difference between the distributions of S-type warps in screened and unscreened regions and it is shown in the right panel of the figure. We found similar results if we use Eq 12 to define warp. In that case  $w_e = 0.5$  kpc separate U-type warps from the rest.

In Figure C3 we show the fraction of galaxies with U-type warps in different environments. We check whether the fraction of normal galaxies and fraction of S-type galaxies have any dependence on their environment and the result is shown in Figure C5. We classify a galaxy as normal if the warp is less than 5%. We find that the fractions of different types of galaxies is independent of their environment. The result is insensitive to the definition of normal galaxy.

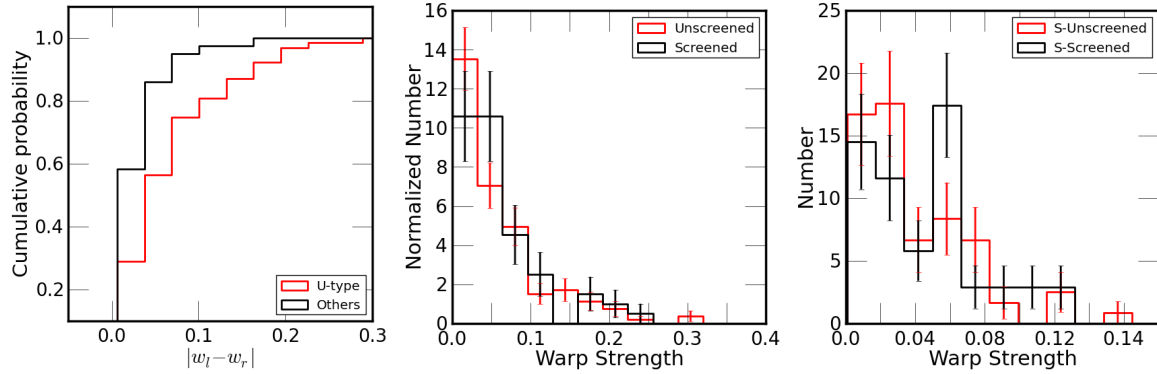


**Figure C4.** Left : The cumulative histogram of  $w_e$  (see text for the definition). The U-type warps can be distinguished with  $w_e > 0.1$ . Middle panel shows the distributions of  $w_e$  in screened and unscreened regions for  $f_{R0} = 2 \times 10^{-7}$ . The right panel shows the distributions of S-type warps in screened and unscreened regions with  $f_{R0} = 2 \times 10^{-7}$ .

Type	$f_{R0}$	Number		$\langle w_1 \rangle$		$\hat{w}_{MG}$	Prediction $\Delta G/G = 1/3, \Delta G/G = 1$
		$N_S$	$N_U$	$w_S$	$w_U$		
All	2e-07	59	158	$0.051 \pm 0.023$	$0.050 \pm 0.014$	$-0.001 \pm 0.027$	
All	1e-06	143	352	$0.038 \pm 0.014$	$0.046 \pm 0.009$	$0.008 \pm 0.017$	
U	2e-07	48	78	$0.031 \pm 0.018$	$0.036 \pm 0.015$	$0.006 \pm 0.023$	$0.003^{0.003}_{0.001}, 0.006^{0.006}_{0.003}$
U	1e-06	89	229	$0.024 \pm 0.012$	$0.029 \pm 0.009$	$0.005 \pm 0.015$	$0.002^{0.002}_{0.001}, 0.004^{0.004}_{0.002}$

	$f_{R0}$	$N_S$	$N_U$	$\langle w_2 \rangle$ (in kpc)		$\hat{w}_{MG}$	Prediction
				$w_S$	$w_U$		
U $h_r = 0.5$ kpc	2e-07	16	11	$0.048 \pm 0.036$	$0.055 \pm 0.051$	$0.007 \pm 0.062$	$0.00 \pm 0.00, 0.00 \pm 0.00$
U $h_r = 1.5$ kpc	2e-07	14	35	$0.151 \pm 0.098$	$0.129 \pm 0.047$	$-0.022 \pm 0.109$	$0.02 \pm 0.02, 0.03 \pm 0.04$
U $h_r = 2.5$ kpc	2e-07	11	24	$0.182 \pm 0.091$	$0.330 \pm 0.104$	$0.148 \pm 0.138$	$0.03 \pm 0.02, 0.07 \pm 0.04$
U $h_r = 3.5$ kpc	2e-07	6	6	$0.312 \pm 0.000$	$0.288 \pm 0.177$	$-0.024 \pm 0.177$	$0.08 \pm 0.06, 0.17 \pm 0.13$
U $h_r = 0.5$ kpc	1e-06	16	13	$0.046 \pm 0.035$	$0.053 \pm 0.041$	$0.006 \pm 0.054$	$0.00 \pm 0.00, 0.00 \pm 0.00$
U $h_r = 1.5$ kpc	1e-06	16	60	$0.094 \pm 0.057$	$0.144 \pm 0.043$	$0.050 \pm 0.071$	$0.01 \pm 0.02, 0.03 \pm 0.03$
U $h_r = 2.5$ kpc	1e-06	15	73	$0.145 \pm 0.074$	$0.215 \pm 0.047$	$0.070 \pm 0.087$	$0.02 \pm 0.02, 0.04 \pm 0.03$
U $h_r = 3.5$ kpc	1e-06	12	50	$0.255 \pm 0.092$	$0.279 \pm 0.066$	$0.024 \pm 0.113$	$0.04 \pm 0.05, 0.09 \pm 0.09$

**Table C1.** Summary of warp tests. The columns are: 1. **Type:** the type of warp included in the analysis. All - included all galaxies, U - used only U-type warps. 2.  $f_{R0}$  - the value of  $f_{R0}$  parameter used to classify screened and unscreened galaxies 3. **Number:** -  $N_S, N_U$  are the number of galaxies in screened and unscreened regions. 4.  $w_S, w_U$  are the average value of the two  $w_1$  or  $w_2$  in screened and unscreened galaxies 5.  $\hat{w}_{MG}$  - estimated warp due to modified gravity. 6. **Prediction:** the theoretical predictions for unscreened galaxies with  $\Delta G/G = 1/3$  and  $\Delta G/G = 1$ . The upper part of the table is for the dimensionless warp parameter  $w_1$  (defined in Eqn. 11) and lower part is for the parameter  $w_2$  (defined in Eqn. 12). In the second part of the table we group U-type galaxies based on their half light radius ( $h_r$ ) to compare the warp. See text for details. The estimated value of  $\hat{w}_{MG}$  is consistent with GR in all cases, but the error bars are too large to detect the MG predictions shown in the last column.

#### APPENDIX D: EXAMPLES OF INTERESTING OBSERVATIONS

We present some examples of optical images (Figures D1 & D2) and rotation curves (Figures D3 & D4) of unscreened galaxies from the literature which look interesting in the context of modified gravity.

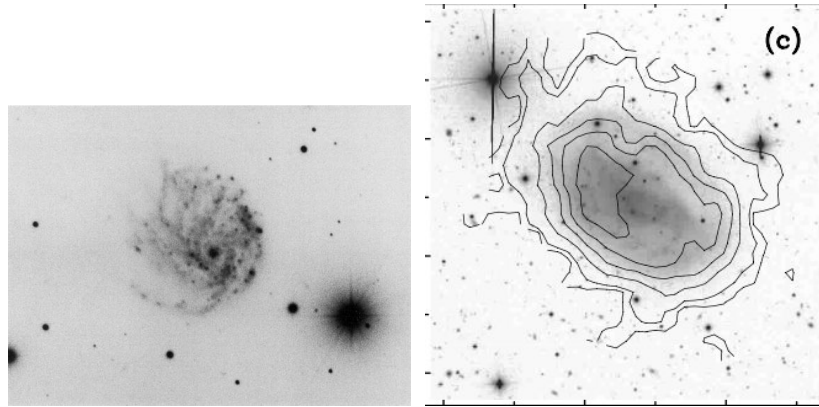


**Figure D1.** *Left panel:* Optical image of dwarf galaxy UGC 3740 which is unscreened for  $f_{R0} = 10^{-6}$ . The galaxy is asymmetric in the optical. The  $H\alpha$  rotation curve also shows strong asymmetry. *Right panel:* Comparison of HI and optical images of UGC 4325. The HI image shows some asymmetry. However, this galaxy does not have any nearby neighbors to which we could attribute an external force. The images are taken from Begum et al. (2008); Swaters et al. (2002)

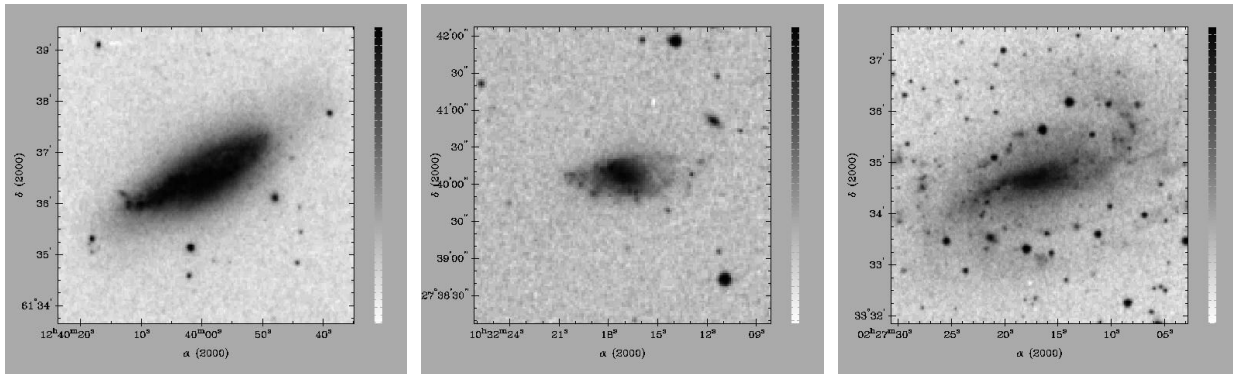


**Figure D2.** Optical images of galaxies with the most asymmetric  $H\alpha$  velocity curves: *Left panel:* UGC 7831 which is unscreened for  $f_{R0} = 10^{-6}$  and shows some warp. *Middle panel:* UGC 5721. *Right panel:* UGC 1913. The images are taken from Begum et al. (2008)

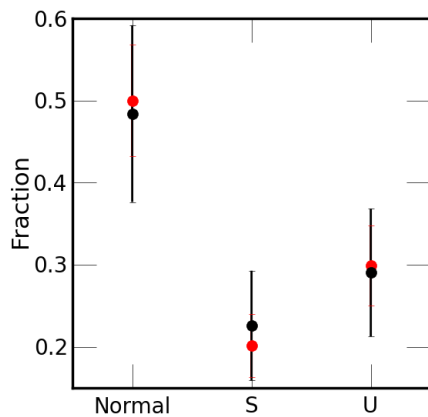


**Figure C5.** The fraction of normal, S-type and U-type galaxies in screened and unscreened regions. We find no noticeable difference between the fraction of different types in screened and unscreened regions. The error in the plots are calculated by assuming Poissonian noise on the number of galaxies.

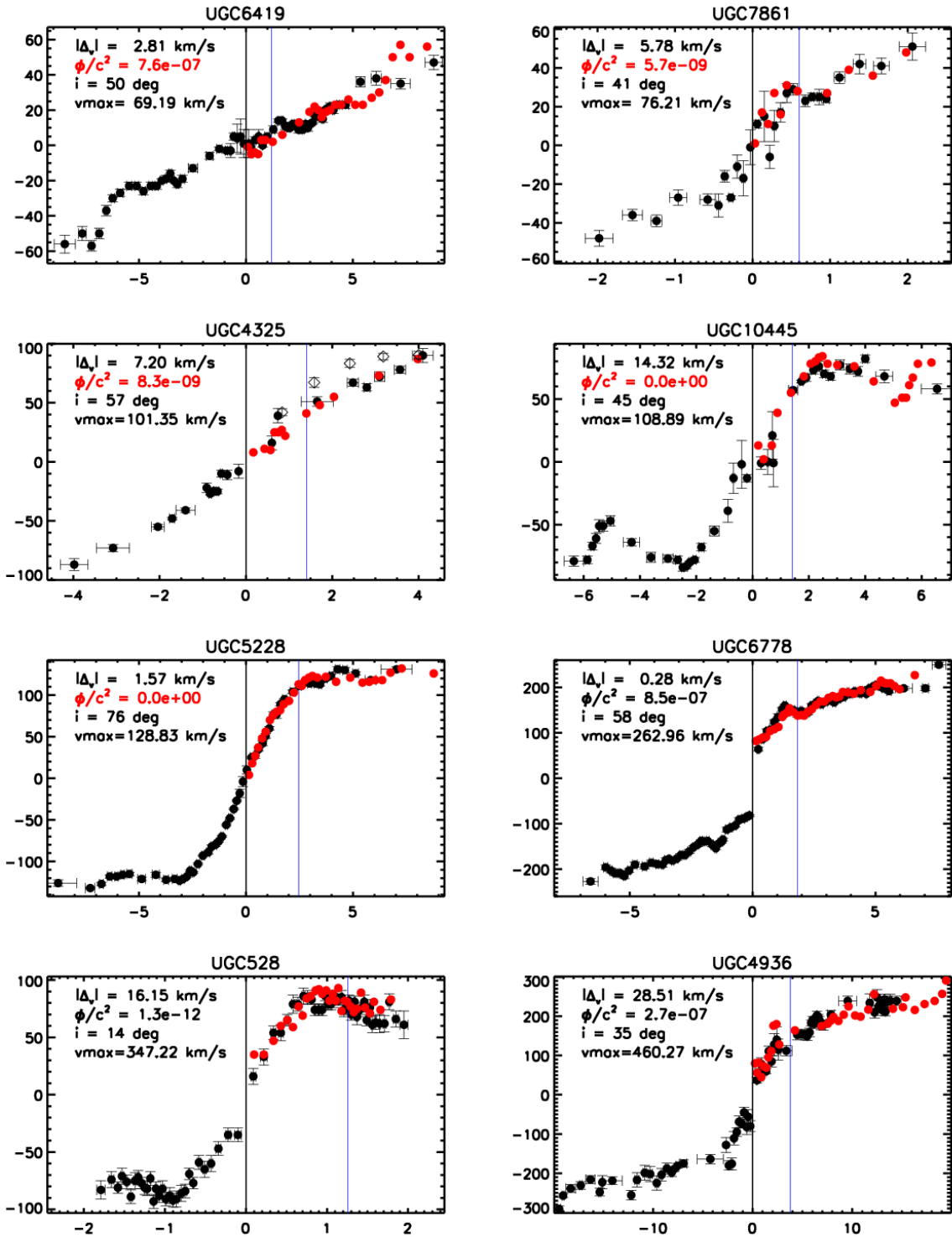


**Figure D3.** Examples of  $H\alpha$  symmetric rotation curves for GHASP galaxies. The x-axis is in kpc, and the y-axis shows the measured rotation velocity in km/s (before correcting for inclination). The left side points of the rotation curves are shown as red points for comparison to the right side. We indicate the name of the galaxy,  $\Delta v$  defined in the text and the external potential due to neighbors within 3 Mpc. The potential is in red if the galaxy is unscreened, and black if it is environmentally screened, for  $f_{R0} = 10^{-6}$ . We label the inclination and the averaged maximum velocity of the galaxy once corrected for inclination. Diamonds show HI curves, when available. The blue vertical lines show the range used to calculate  $\Delta v$ , based on its half-light radius. Note that for UGC 4325 the velocity in HI is larger than in  $H\alpha$ .

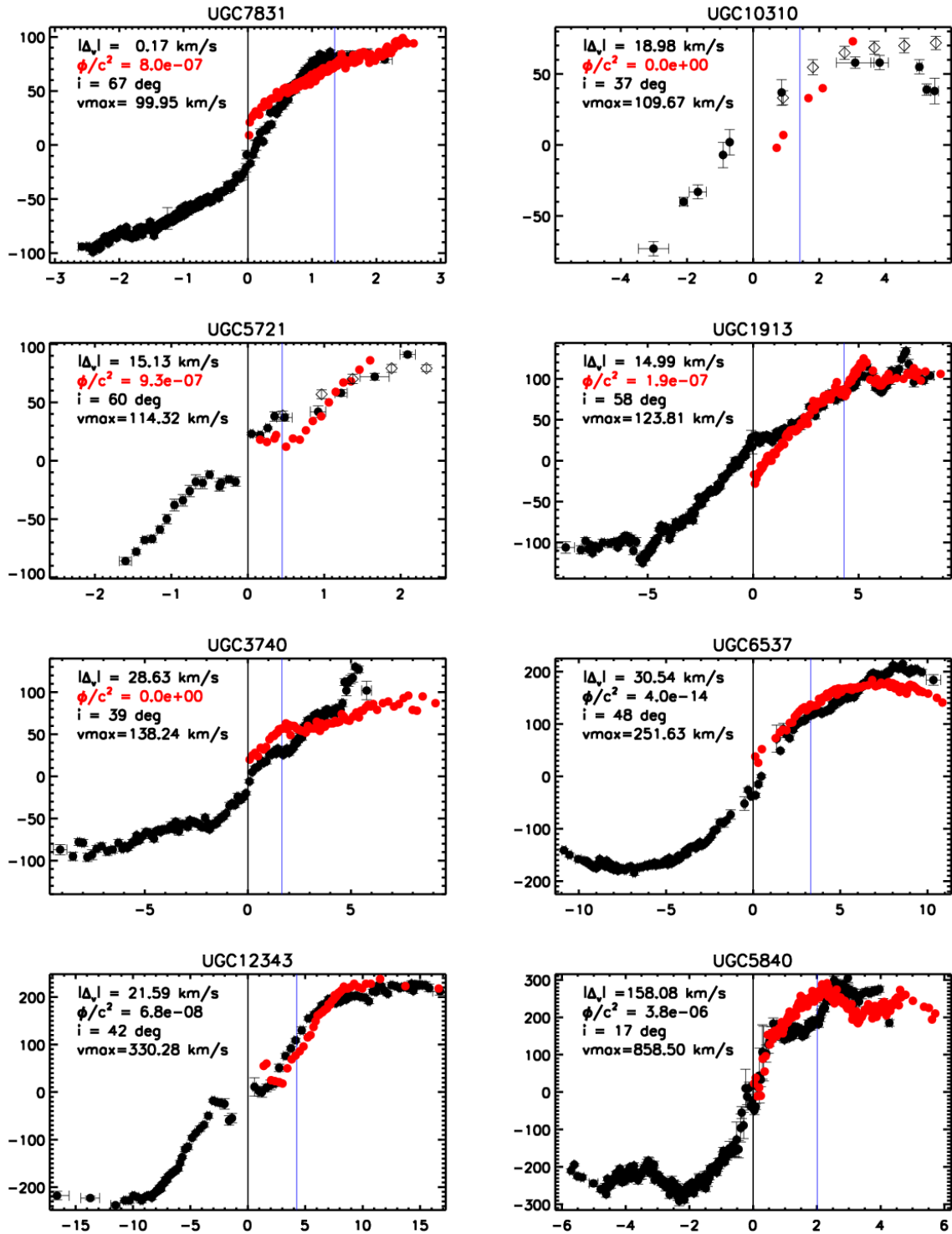


**Figure D4.** Same as Figure D3 for smoothly asymmetric curves, selected visually. These slow varying asymmetries could be created by modified gravity.